IMMUNOLOGY

Cbl-b mitigates the responsiveness of naive CD8$^+$ T cells that experience extensive tonic T cell receptor signaling

Joel Eggert[1], Wendy M. Zinzow-Kramer[1], Yuesong Hu[2], Elizabeth M. Kolawole[3], Yuan-Li Tsai[4], Arthur Weiss[4], Brian D. Evavold[3], Khalid Salaita[2], Christopher D. Scharer[5], Byron B. Au-Yeung[1]*

Naive T cells experience tonic T cell receptor (TCR) signaling in response to self-antigens presented by major histocompatibility complex (MHC) in secondary lymphoid organs. We investigated how relatively weak or strong tonic TCR signals influence naive CD8$^+$ T cell responses to stimulation with foreign antigens. The heterogeneous expression of Nur77-GFP, a transgenic reporter of tonic TCR signaling, in naive CD8$^+$ T cells suggests variable intensities or durations of tonic TCR signaling. Although the expression of genes associated with acutely stimulated T cells was increased in Nur77-GFP^{HI} cells, these cells were hyporesponsive to agonist TCR stimulation compared with Nur77-GFP^{LO} cells. This hyporesponsiveness manifested as diminished activation marker expression and decreased secretion of IFN-γ and IL-2. The protein abundance of the ubiquitin ligase Cbl-b, a negative regulator of TCR signaling, was greater in Nur77-GFP^{HI} cells than in Nur77-GFP^{LO} cells, and Cbl-b deficiency partially restored the responsiveness of Nur77-GFP^{HI} cells. Our data suggest that the cumulative effects of previously experienced tonic TCR signaling recalibrate naive CD8$^+$ T cell responsiveness. These changes include gene expression changes and negative regulation partially dependent on Cbl-b. This cell-intrinsic negative feedback loop may enable the immune system to restrain naive CD8$^+$ T cells with higher self-reactivity.

INTRODUCTION

The activation of T cell–mediated immune responses is associated with sustained, robust signal transduction triggered by the T cell antigen receptor (TCR) (*1*). Activating TCR signals induces changes in T cell metabolism, cytoskeleton arrangements, and gene expression (*1*). Transcription of immediate-early genes occurs rapidly in response to robust TCR stimuli and includes transcription factors of the Jun/Fos family and Nur77, an orphan nuclear receptor encoded by *Nr4a1* (*2*). However, T cells also constitutively experience TCR signals stimulated by self-peptides presented by major histocompatibility complex (self-pMHC) in secondary lymphoid organs (SLOs) (*3*). These tonic or basal TCR signals induce constitutive tyrosine phosphorylation of immunoreceptor tyrosine–based activation motifs within the TCR complex and association of the tyrosine kinase ZAP-70 with the CD3 ζ-chain even in naive T cells (*4*, *5*). TCR:self-pMHC signals do not typically produce a cellular phenotype associated with an effector T cell (*3*). However, tonic TCR signals can alter chromatin accessibility and influence the expression of several genes at the transcriptional or the protein level in T cells (*6*–*9*). This feature of tonic TCR signaling also raises the possibility that variable gene expression patterns in response to tonic TCR signaling result in functional heterogeneity within the naive T cell population (*10*, *11*). How the intensity of tonic TCR signals helps shape the responsiveness of naive T cells to subsequent foreign antigen stimulation remains unresolved (*3*).

The immediate downstream effects of strong tonic TCR signals, such as CD3 ζ-chain phosphorylation and ZAP-70 recruitment to the TCR complex, are transient events (*4*). For example, the loss of ζ-chain phosphorylation and the dissociation of ZAP-70 from the TCR complex is evident in peripheral blood T cells compared with cells harvested from SLOs (*4*). Hence, the expression of proteins induced by TCR signaling, such as Nur77 and CD5, are surrogate markers of tonic TCR signaling (*3*). Transgenic reporters of *Nr4a* family genes, including *Nr4a1* and *Nr4a3*, can provide fluorescence-based readouts of TCR signaling (*12*). The Nur77-GFP reporter transgene consists of enhanced green fluorescent protein (GFP) driven by the promoter and enhancer elements of the *Nr4a1* gene (*13*, *14*). TCR stimulation induces *Nr4a1* gene transcription and Nur77-GFP reporter expression in relative proportion to TCR signal strength. For example, the mean fluorescence intensity (MFI) of Nur77-GFP expressed by acutely stimulated T cells decreases with diminishing pMHC affinity (*13*, *15*). Furthermore, Nur77-GFP expression is relatively insensitive to constitutively active signal transducer and activator of transcription 5 (STAT5) or inflammatory signals, suggesting that reporter transgene expression is activated selectively by TCR stimulation in T cells (*13*). TCR-induced Nur77-GFP expression is also sensitive to inhibitors of TCR signaling proteins, including the tyrosine kinase ZAP-70 (*16*).

Naive T cells express Nur77-GFP in response to tonic or basal TCR signals from self-pMHC interactions in SLOs in unchallenged mice housed under specific pathogen–free conditions (*13*, *17*, *18*). In this study, we investigated the functional responsiveness of naive CD8$^+$ T cells that expressed relatively low or high levels of Nur77-GFP. Naive CD8$^+$ T cells expressing the highest levels of Nur77-GFP exhibited relative hyporesponsiveness to stimulation with agonist TCR ligands and differential gene expression, including genes potentially inhibiting T cell activation. We found that naive CD8$^+$ T cells expressing high levels of Nur77-GFP from mice lacking Cbl-b exhibited partially rescued responsiveness to TCR stimulation. Together, these findings suggest a model in which naive CD8$^+$ T cells adapt to high levels of tonic TCR signaling through negative regulation that limits T cell responsiveness.

[1]Division of Immunology, Lowance Center for Human Immunology, Department of Medicine, Emory University, Atlanta, GA 30322, USA. [2]Department of Chemistry, Emory University, Atlanta, GA 30322, USA. [3]Department of Pathology, University of Utah School of Medicine, Salt Lake City, UT 84112, USA. [4]Rosalind Russell and Ephraim P. Engleman Rheumatology Research Center, Departments of Medicine and of Microbiology and Immunology, University of California, San Francisco, San Francisco, CA 94143, USA. [5]Department of Microbiology and Immunology, Emory University, Atlanta, GA 30322, USA.
*Corresponding author. Email: byron.au-yeung@emory.edu

RESULTS

Naive CD8$^+$ T cells experience variable strengths of tonic TCR signaling

We first sought to investigate the diversity of Nur77-GFP expression in the CD8$^+$ T cell population. TCR polyclonal naive CD8$^+$ and CD4$^+$ T cells, as defined by their CD44^{LO} CD62L^{HI} cell surface phenotype, expressed Nur77-GFP in a range spanning over three orders of magnitude (fig. S1A). The Nur77-GFP intensities of naive CD4$^+$ and CD8$^+$ T cells were higher than that in nontransgenic T cells but lower compared with that in CD4$^+$ Foxp3$^+$ regulatory T cells (fig. S1A), a T cell population that expresses TCRs with higher self-reactivity (*19*–*21*). We next compared two subpopulations of naive CD8$^+$ T cells: the 10% of naive CD8$^+$ T cells with the highest Nur77-GFP fluorescence intensity (GFP^{HI}) and the 10% of naive CD8$^+$ T cells with the lowest Nur77-GFP fluorescence intensity (GFP^{LO}). Levels of surface TCRβ and CD8α on GFP^{HI} and GFP^{LO} cells were largely overlapping or slightly reduced in GFP^{HI} cells (Fig. 1A). We also did not detect differences in surface and intracellular TCRβ staining intensity between naive polyclonal GFP^{LO} and GFP^{HI} cells (fig. S1, B and C), suggesting a lack of correlation between Nur77-GFP reporter expression and total TCR levels. The magnitude of CD5 surface expression correlates with TCR reactivity to self-pMHC (*22*–*26*). CD5 staining intensity was increased in naive, polyclonal GFP^{HI} CD8$^+$ T cells, in agreement with previous results and consistent with the concept that the intensity of CD5 and Nur77-GFP expression can reflect the strength of tonic TCR signaling [fig. S1D and (*27*)]. Naive GFP^{HI}

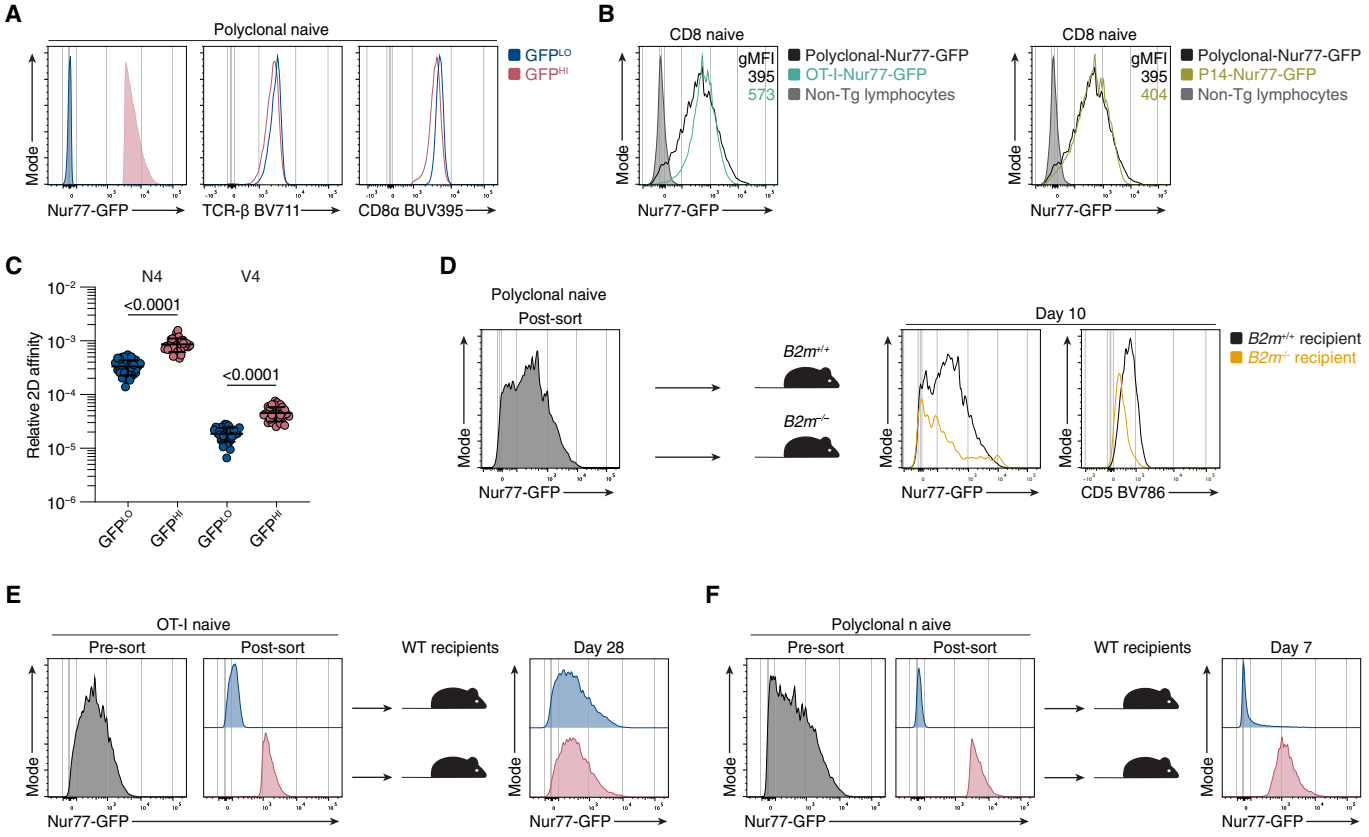

Fig. 1. The intensity of tonic TCR signaling in naive CD8$^+$ T cells is heterogeneous. (**A**) Overlaid histogram (left) depicts GFP fluorescence for GFP^{LO} and GFP^{HI} cells in the spleen. GFP^{LO} cells are the 10% of cells with the lowest (blue) GFP fluorescence intensity, whereas GFP^{HI} cells are the 10% of cells with the highest (red) GFP fluorescence intensity. Histograms (middle and right) show expression of TCRβ and CD8α by polyclonal naive GFP^{LO} and GFP^{HI} CD8$^+$ T cells. (**B**) Polyclonal (black) and OT-I-*Trac*$^{-/-}$ (cyan) T cells were gated on CD44^{LO} CD62L^{HI} CD8$^+$ cells (left), and P14 T cells (green) were gated on CD44^{LO} CD62L^{HI} Vα2$^+$ CD8$^+$ cells (right). Representative flow cytometry plots of Nur77-GFP fluorescence of splenic naive polyclonal or TCR-transgenic CD8$^+$ T cells. Gray histograms depict nontransgenic lymphocytes, and the numbers indicate the geometric mean fluorescence intensity (gMFI) calculated for the whole population. (**C**) Graph displays the relative two-dimensional affinity of naive GFP^{LO} and GFP^{HI} OT-I cells to N4 or V4 peptide/H2K^b monomers. Each symbol represents one cell with a total of 33 or 34 cells from three independent experiments. Bars depict the mean, and error bars show ±SD. Statistical testing was performed by unpaired two-tailed Student's *t* test. (**D**) Naive polyclonal CD8$^+$ T cells (~2.5 × 10^6) were adoptively transferred into *B2m*$^{+/+}$ or *B2m*$^{-/-}$ recipients. Histogram (left) shows the Nur77-GFP fluorescence intensity of FACS-sorted naive polyclonal CD8$^+$ T cells. Histograms (middle and right) show Nur77-GFP fluorescence and CD5 staining intensity of T cells transferred into *B2m*$^{+/+}$ (black) or *B2m*$^{-/-}$ (orange) recipients 10 days after transfer. (**E**) GFP^{LO} or GFP^{HI} OT-I cells (~1.5 × 10^6) were adoptively transferred into separate WT congenic recipients. GFP^{LO} and GFP^{HI} cells were sorted from the 20% of cells with the lowest and highest Nur77-GFP fluorescence intensity, respectively. Histograms show the Nur77-GFP fluorescence intensity of total naive OT-I cells (left) or FACS-sorted GFP^{LO} and GFP^{HI} cells (middle). Histogram (right) shows Nur77-GFP fluorescence of transferred T cells 4 weeks after transfer. (**F**) A total of 5 × 10^5 GFP^{LO} or GFP^{HI} polyclonal CD8$^+$ T cells were adoptively transferred into separate WT congenic recipients. Donor cells were gated on naive CD8$^+$ T cells, the congenic marker expression (E and F), and, in addition, TCR-β$^+$ cells (D). Histograms show the Nur77-GFP fluorescence intensity of total CD8$^+$ T cells (left) or FACS-sorted GFP^{LO} and GFP^{HI} cells (middle). Histogram (right) shows Nur77-GFP fluorescence of transferred T cells 7 days after transfer. Data in (B) represent two independent experiments with *n* = 2 mice. Data in (D) to (F) represent two independent experiments with *n* = 2 mice for each group. Data in (A) and (C) represent three independent experiments with *n* = 3 mice.

$CD8^+$ T cells were $CD44^{LO}$ $CD62L^{HI}$, consistent with a naive surface marker phenotype. However, within the naive $CD8^+$ population, GFP^{HI} cells exhibited increased CD44 staining intensity relative to GFP^{LO} cells (fig. S1E). This result is consistent with a previous study showing that $CD5^{HI}$ naive $CD8^+$ T cells express higher levels of CD44 than $CD5^{LO}$ cells (*27*).

We hypothesized that restricting the repertoire to a single TCR specificity would decrease the heterogeneity of Nur77-GFP expression in a TCR-transgenic population. To test the influence of TCR specificity on the distribution of Nur77-GFP expression, we compared the intensity and distribution of Nur77-GFP among naive polyclonal, OT-I, and P14 TCR-transgenic populations. The geometric MFI (gMFI) of Nur77-GFP in naive $CD44^{LO}$ $CD62L^{HI}$ OT-I cells was higher than that in polyclonal naive $CD8^+$ cells, whereas P14 cells and polyclonal cells had similar gMFI values (Fig. 1B and fig. S1F). These results suggested that TCR specificity can influence the intensity of TCR signaling experienced by individual T cells. We also detected similar Nur77-GFP fluorescence intensities in $Trac^{-/-}$ and $Trac^{+/-}$ P14 cells, suggesting that endogenous TCR α-chain (*Trac*) expression in naive TCR-transgenic cells does not affect Nur77-GFP fluorescence intensity (fig. S1G).

Increased Nur77-GFP expression could reflect more intense or frequent tonic TCR signals. We hypothesized that Nur77-GFP expression in naive OT-I cells would correlate with the relative TCR:pMHC two-dimensional (2D) affinity. To test this hypothesis, we used a 2D micropipette adhesion frequency (2D-MP) assay (*28*), which measures the relative affinity of OT-I TCRs for pMHC in 2D membrane environments. We compared naive GFP^{LO} and GFP^{HI} cells that expressed the OT-I TCR and were deficient for the endogenous TCR α chain to prevent endogenous TCR recombination. Furthermore, we excluded $Qa2^{LO}$ recent thymic emigrants (RTEs), which were more abundant in 6- to 13-week-old OT-I or P14 TCR-transgenic mice but present at low frequencies in wild-type (WT) mice (fig. S1, H and I). RTEs continue to undergo maturation and exhibit diminished functional responses compared with mature T cells (*29*). Sorted naive GFP^{LO} and GFP^{HI} OT-I cells were brought into contact with human red blood cells (RBCs) coated with the cognate SIINFEKL (N4) peptide or the weaker affinity SIIVFEKL (V4) peptide presented by $H2K^b$, and RBC elongation was detected as a measure of an adhesion event (*30*). By calculating the adhesion frequency from a set of different T cell:RBC interaction times, the generated binding curve is used to calculate 2D affinity (*31*). GFP^{HI} naive OT-I cells exhibited an increase in relative TCR:pMHC 2D affinity for both N4 and V4 pMHC antigens compared with GFP^{LO} cells (Fig. 1C). These data suggest that higher relative 2D affinity interactions with N4, V4, and possibly to self-pMHC correlate with increased steady-state Nur77-GFP expression. This result is consistent with a previous study from our laboratory that revealed a positive correlation between Nur77-GFP expression in naive $CD4^+$ OT-II cells and the relative 2D affinity to ovalbumin (OVA) peptide/MHC (*7*).

We hypothesized that Nur77-GFP expression in naive $CD8^+$ T cells depends on exposure to pMHC. To test this hypothesis, we adoptively transferred naive polyclonal $CD8^+$ T cells into $B2m^{-/-}$ or $B2m^{+/+}$ recipients for 10 days. The $CD8^+$ T cells transferred into $B2m^{-/-}$ recipients exhibited a reduction in Nur77-GFP fluorescence and CD5 staining intensities (Fig. 1D). These results suggest that Nur77-GFP expression in naive $CD8^+$ T cells depended on continuous exposure to pMHC and its abundance. Accordingly, previous studies showed that Nur77-GFP expression in naive $CD4^+$ T cells also requires continuous exposure to pMHC (*13*, *18*). Hence, Nur77-GFP expression in naive T cells reflects the frequency and intensity of relatively recently experienced tonic TCR signaling.

We adoptively transferred GFP^{LO} and GFP^{HI} naive OT-I cells into congenic lymphoreplete recipients to determine whether the bias in Nur77-GFP expression was sustained beyond several half-lives of GFP protein in a TCR-transgenic population. Four weeks after transfer, the distribution of Nur77-GFP fluorescence overlapped completely (Fig. 1E). These results suggest that biases in Nur77-GFP expression in a naive TCR-transgenic population shift over extended periods. We next investigated how Nur77-GFP expression changes in naive polyclonal $CD8^+$ T cells over several days by adoptively transferring GFP^{LO} or GFP^{HI} naive polyclonal $CD8^+$ T cells into congenic lymphoreplete recipients for 1 week (Fig. 1F). Donor GFP^{LO} cells tended to sustain low Nur77-GFP intensity, although weak affinity antigens can induce OT-I cells to increase expression of Nur77-GFP in less than 8 hours (*13*). These results suggested that polyclonal GFP^{LO} cells tended to experience weak tonic TCR signals over 1 week (Fig. 1F). GFP^{HI} naive donor T cells also sustained relatively high Nur77-GFP expression (Fig. 1F), although this phenotype could be partially due to the reported 26- to 54-hour half-life of enhanced GFP protein (*32*, *33*). These results are consistent with previous work showing that sorted TCR polyclonal $CD5^{LO}$ and $CD5^{HI}$ naive $CD4^+$ and $CD8^+$ T cells maintain skewed CD5 expression more than 4 weeks after adoptive transfer into lymphoreplete recipients (*22*, *27*). Hence, differences in TCR specificities may enable biased Nur77-GFP transgene expression in naive polyclonal T cells for more extended time periods.

We next asked whether Nur77-GFP expression by naive $CD8^+$ T cells varied in different anatomical locations. The intensity or distribution of Nur77-GFP expression in naive $CD8^+$ T cells from different SLOs, such as the spleen, mesenteric lymph nodes, and Peyer's patches, did not differ (fig. S1J). Subsequently, we queried whether the location within the spleen could contribute to heterogeneous Nur77-GFP expression in naive $CD8^+$ T cells. To compare the Nur77-GFP distribution of T cells located in the more vascularized red pulp compared to the white pulp of the spleen, we performed intravascular labeling with fluorescently labeled anti-CD45 antibodies 3 min before euthanasia. We detected largely overlapping Nur77-GFP intensities for naive polyclonal $CD8^+$ T cells labeled with anti-CD45 and cells not labeled with anti-CD45, which we interpreted to represent cells located in the red and white pulp, respectively (fig. S1K). These results suggest that GFP^{LO} and GFP^{HI} cells were not skewed in their distribution between the red or white pulp in the spleen or the SLOs we analyzed. Together, we interpret Nur77-GFP fluorescence intensity in naive $CD8^+$ T cells to reflect the strength of recently experienced tonic TCR signals. Factors that influence tonic TCR stimulation, such as TCR specificity, relative 2D affinity, and frequency and duration of TCR stimulations, can influence the intensity of Nur77-GFP expression in naive T cells.

Naive $CD8^+$ T cells that experience extensive tonic TCR signaling are hyporesponsive to TCR stimulation

To analyze the functional responsiveness of naive T cells expressing different levels of Nur77-GFP, we isolated three subpopulations (GFP^{LO}, GFP^{MED}, and GFP^{HI}) from naive, polyclonal $CD8^+$ T cells (Fig. 2A and fig. S2A). After 24 hours of stimulation with soluble anti-CD3 antibodies and splenocyte antigen-presenting

cells (APCs), we labeled cells with an interferon-γ (IFN-γ) catch reagent consisting of an anti-CD45 antibody conjugated with an anti–IFN-γ antibody (*34*, *35*). After a 45-min secretion period at 37°C, we labeled the cells with a second anti–IFN-γ antibody to visualize secreted and "captured" IFN-γ (*35*). The frequency of IFN-γ–secreting cells in the GFP^{LO} subpopulation was more than twofold higher compared with the GFP^{MED} population and more than 30-fold higher relative to the GFP^{HI} population (Fig. 2, B and C). Hence, there was an apparent inverse correlation between the intensity of steady-state GFP expression and the magnitude of anti-CD3–induced IFN-γ secretion. Although cytokine production increases after T cells have undergone cell division, naive T cells can produce effector cytokines within 24 hours of stimulation and before cell division (*23*, *36*–*43*). We also detected a similar inverse correlation between Nur77-GFP expression and IFN-γ secretion in naive GFP^{LO} and GFP^{HI} P14 TCR-transgenic cells stimulated with GP33 peptide and splenocyte APCs (fig. S2, B and C) (*44*).

To determine whether GFP^{LO}, GFP^{MED}, and GFP^{HI} cells similarly increased expression of receptors associated with acute T cell activation, we analyzed the expression of the activation markers CD25, CD69, and transferrin receptor (CD71), in addition to the Nur77-GFP reporter. All three populations expressed Nur77-GFP and CD69 above baseline levels (Fig. 2D and fig. S2D). However, on average, GFP^{LO} cells expressed higher levels of CD69 than GFP^{MED} and GFP^{HI} cells (Fig. 2D). Similarly, higher frequencies of the GFP^{LO} population expressed higher levels of CD25 and CD71 compared with GFP^{HI} cells (Fig. 2D). After stimulation, the sorted GFP^{LO}, GFP^{MED}, and GFP^{HI} populations each expressed similar levels of Nur77-GFP at the 24-hour end point (Fig. 2D).

To test whether GFP^{LO} and GFP^{HI} cells exhibited differences in survival after stimulation, we quantified the proportion of viable $CD8^+$ T cells after the 24-hour stimulation period. GFP^{HI} cells had a 1.5-fold reduction in the percentage of viable cells compared with GFP^{LO} cells (fig. S2E). Hence, GFP^{HI} cell viability is decreased relative

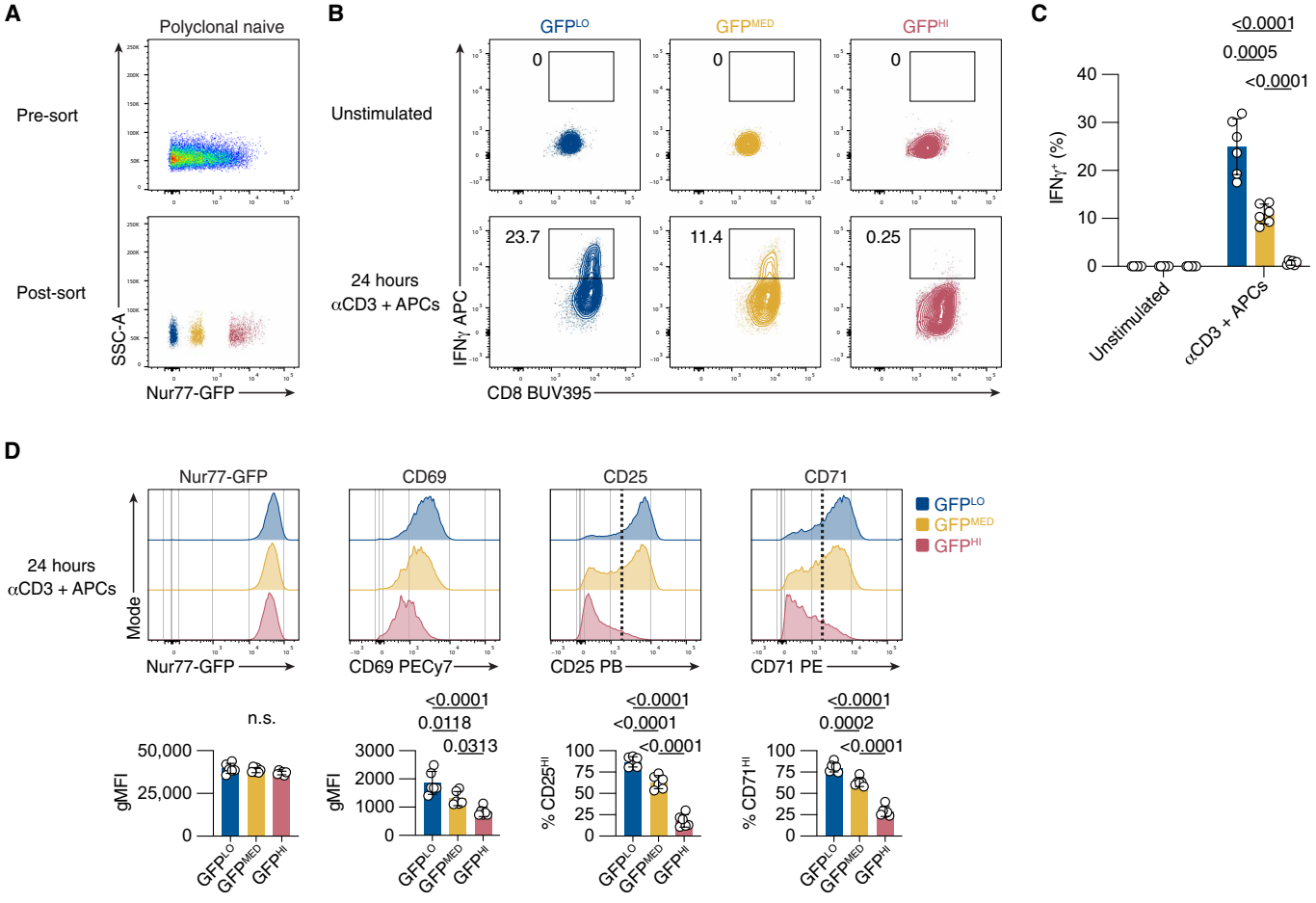

Fig. 2. Extensive tonic TCR signaling negatively correlates with naive, polyclonal CD8 T cell responsiveness. (**A**) Representative flow cytometry plots show Nur77-GFP fluorescence of total $CD8^+$ cells (top) and sorted GFP^{LO}, GFP^{MED}, and GFP^{HI} naive, polyclonal CD8 T cell populations (bottom). (**B**) Contour plots depict CD8 and IFN-γ expression by unstimulated and stimulated viable polyclonal $CD8^+$ T cells after a 45-min IFN-γ secretion assay. Numbers indicate the percentage of cells within the indicated gates. (**C**) Bar graph displays the frequencies of GFP^{LO}, GFP^{MED}, and GFP^{HI} IFN-γ–secreting cells. Cells were either unstimulated or stimulated for 24 hours with anti-CD3 (0.25 μg/ml) and APCs before the secretion assay. (**D**) Histograms show expression of the indicated activation markers of cells stimulated for 24 hours with anti-CD3 (0.25 μg/ml) and APCs. Cells were gated on viable $CD8^+$ T cells. Bar graphs display the gMFI for Nur77-GFP and CD69 or the frequency of marker-positive cells for CD25 and CD71 (as indicated by the dotted line in the histogram). Data in (A) to (D) represent three independent experiments with $n = 6$ mice. In (C) and (D), bars depict means, error bars show ±SD, and each symbol represents one mouse. For (C), $P < 0.0001$ by one-way analysis of variance (ANOVA), followed by Tukey's multiple comparisons test. For (D), $P < 0.0001$ for CD69, CD25, and CD71 by one-way ANOVA, followed by Tukey's multiple comparisons test. n.s., not significant.

to GFP^{LO} cell viability after TCR stimulation. We next asked whether GFP^{LO} and GFP^{HI} cells exhibited differences in cell division. We hypothesized that more extensive tonic TCR signaling would result in delayed or reduced cell division upon stimulation of naive CD8$^+$ T cells. We sorted naive GFP^{LO} and GFP^{HI} polyclonal T cells and assessed in vitro proliferation after stimulation with anti-CD3 antibodies and APCs (fig. S2F). Three days after stimulation, the proliferation index (the average number of divisions of cells that divided at least once) of GFP^{LO} cells was greater than that of GFP^{HI} cells (fig. S2G). This result suggests that extensive tonic TCR signaling inhibits the proliferation of naive CD8$^+$ T cells under the conditions tested.

We further hypothesized that naive GFP^{LO} cells might have a competitive advantage during the early phase of an immune response in vivo relative to GFP^{HI} cells. To investigate this hypothesis, we sorted GFP^{LO} and GFP^{HI} subpopulations of naive CD44^{LO} CD62L^{HI} Qa2^{HI} Vα2^{HI} P14 TCR-transgenic cells (fig. S2H). We cotransferred an equal number of congenically distinct GFP^{LO} and GFP^{HI} cells (3000 each) into WT recipients to analyze the ratiometric difference between the two populations after a viral infection. Five days after lymphocytic choriomeningitis virus (LCMV) infection, the ratio between GFP^{LO} and GFP^{HI} cells in the spleen was skewed about 1.6-fold in favor of GFP^{LO} cells (fig. S2I). Hence, GFP^{LO} cells have a slight competitive advantage over GFP^{HI} cells in the early phase of an immune response that persists through multiple rounds of cell division.

We next compared the cellular responses of GFP^{LO} and GFP^{HI} naive CD8$^+$ OT-I TCR-transgenic cells to titrated doses of peptide and with altered peptides that vary in affinity for the OT-I TCR. We postulated that GFP^{HI} T cells exhibited decreased responsiveness for pMHC at low concentrations or weak affinity pMHC ligands. We sorted GFP^{LO} and GFP^{HI} naive T cells with a CD8$^+$ CD44^{LO} CD62L^{HI} Qa2^{HI} phenotype from OT-I *Trac*$^{-/-}$ TCR-transgenic mice (Fig. 3A) and assessed the increased expression of CD25 and CD69 after stimulation for 16 hours with APCs and the cognate N4 peptide. The dose-response curve of GFP^{HI} cells was shifted further to the right compared with GFP^{LO} cells, indicating a relative reduction in CD25 and CD69 expression. The calculated median effective concentration (EC$_{50}$) value for GFP^{LO} cells was 1.4-fold lower than for GFP^{HI} cells (Fig. 3B and fig. S3, A and B). These results suggest that GFP^{HI} cells exhibit reduced responsiveness to a high-affinity antigen under nonsaturating antigen doses.

To test whether extensive tonic TCR signaling affected the responsiveness to antigen affinity, we also stimulated OT-I cells with the SIIQFERL (Q4R7) altered peptide, which has reduced affinity for the OT-I TCR relative to the N4 peptide (*45*). The Q4R7 dose-response curve of GFP^{HI} cells was increasingly shifted to the right relative to the N4 dose-response curve and to Q4R7-stimulated GFP^{LO} cells. The calculated EC$_{50}$ value for GFP^{LO} cells was 2.9-fold

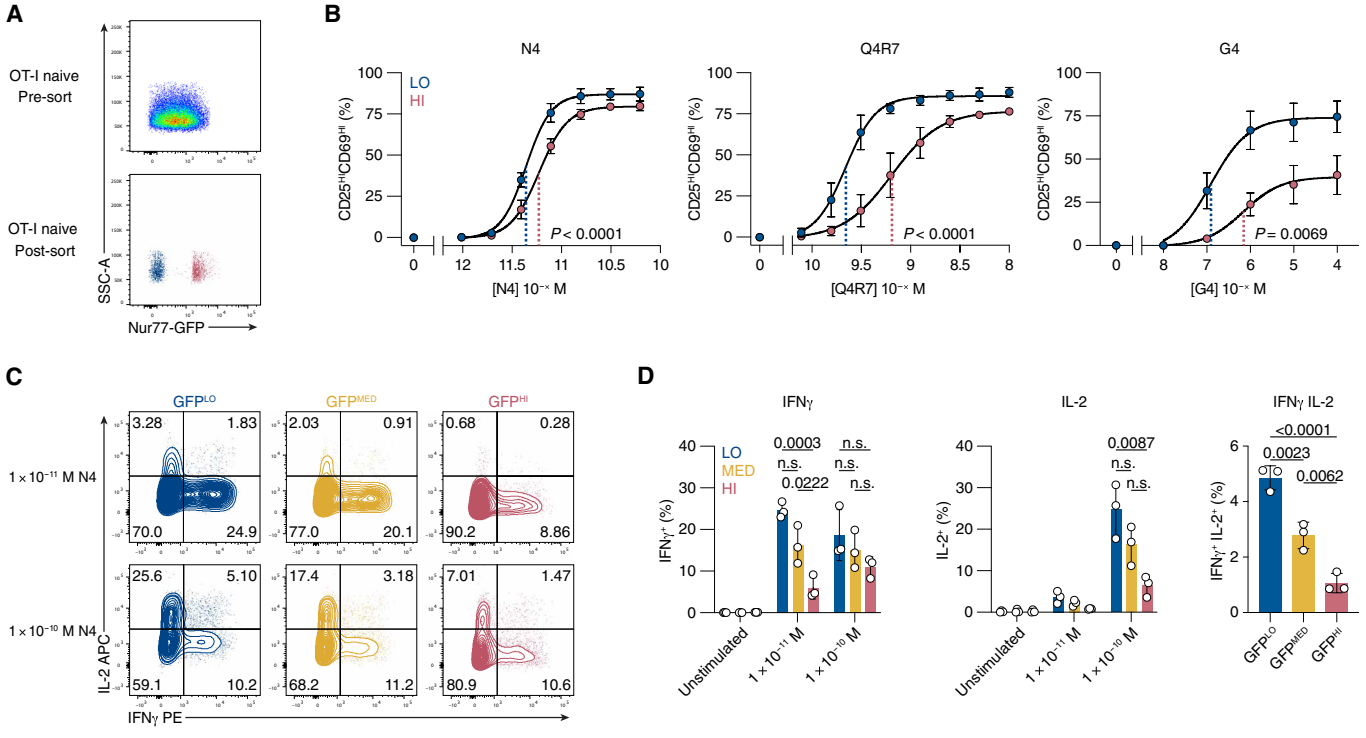

Fig. 3. Extensive tonic TCR signaling correlates negatively with naive OT-I cell responsiveness. (**A**) Representative flow cytometry plots show Nur77-GFP fluorescence of total cells (top) and sorted GFP^{LO} and GFP^{HI} naive CD8 T cell populations (bottom) from OT-I-Nur77-GFP-*Trac*$^{-/-}$ mice. (**B**) Graphs show the frequencies of CD25^{HI}CD69^{HI} cells after 16 hours of stimulation with indicated peptide concentrations and APCs. Plotted are mean values fitted by nonlinear regression curves. The dotted lines indicate the $\log_{10}$ EC$_{50}$ for GFP^{LO} (blue) and GFP^{HI} (red) cells. *P* values were generated by Student's *t* tests for the $\log_{10}$ EC$_{50}$ (the null hypothesis being that the $\log_{10}$ EC$_{50}$ is the same for the two populations). (**C**) Contour plots depict viable CD8$^+$ T cells after a 45-min assay of the secretion of IFN-γ and IL-2 from stimulated (16 hours) OT-I CD8$^+$ T cells. (**D**) Bar graphs show the frequencies of IFN-γ, IL-2, or IFN-γ and IL-2–secreting cells after 16 hours of stimulation with indicated N4 peptide concentrations and APCs or unstimulated control. Data in (A) to (D) represent three independent experiments with $n = 3$ biological replicates. In (B) and (D), bars depict means, error bars show ±SD, and in (D), each symbol represents one biological replicate. In (D), $P = 0.0004$ by two-way analysis of variance (ANOVA) (left) and $P = 0.0107$ (middle) or $P = 0.0001$ (right) by one-way ANOVA followed by Tukey's multiple comparisons test. n.s., not significant.

lower than for GFP^{HI} cells (Fig. 3B and fig. S3B). Upon stimulation with the weak agonist peptide SIIGFEKL (G4), the dose-response curve also shifted to the right for GFP^{HI} cells. The calculated EC_{50} value for GFP^{LO} cells was 5.8-fold lower than for GFP^{HI} cells (Fig. 3B and fig. S3B). These results indicated that higher levels of accumulated TCR signaling from self-pMHC in naive CD8$^+$ T cells resulted in hyporesponsiveness to subsequent stimulation.

We next asked whether GFP^{LO} and GFP^{HI} OT-I cells exhibited differences in TCR-induced cytokine secretion. We hypothesized that GFP^{HI} cells would exhibit decreased interleukin-2 (IL-2) and IFN-γ secretion relative to GFP^{MED} and GFP^{LO} cells. GFP^{LO}, GFP^{MED}, and GFP^{HI} naive OT-I cells were sorted and stimulated for 16 hours with an N4 peptide concentration (1×10^{-11} M) that was on the linear range of the curve for CD25 and CD69 expression, followed by IL-2 and IFN-γ capture assays (Fig. 3, C and D). The frequency of IFN-γ–secreting GFP^{LO} OT-I cells was approximately fourfold higher relative to GFP^{HI} cells (Fig. 3, C and D). The frequency of IL-2–secreting cells was below 5% for all populations at a dose of 1×10^{-11} M N4 peptide (Fig. 3, C and D). To induce more robust IL-2 secretion, we stimulated the three populations with a 10-fold higher dose of N4 peptide (1×10^{-10} M). At this dose, there was comparable IFN-γ secretion (Fig. 3, C and D). However, the frequency of IL-2–secreting GFP^{LO} cells was approximately fourfold higher relative to that of GFP^{HI} cells (Fig. 3, C and D). Similarly, the frequency of cells that secreted both IL-2 and IFN-γ was about 1.7-fold higher in GFP^{LO} cells compared with GFP^{MED} cells and more than fourfold higher in GFP^{LO} relative to GFP^{HI} cells (Fig. 3, C and D). Hence, there was a dose-dependent, inverse correlation between Nur77-GFP expression in naive CD8$^+$ T cells and cytokine secretion in response to subsequent TCR stimulation.

CD8$^+$ GFP^{HI} cells exhibit attenuated Ca^{2+} flux responses and exert reduced mechanical forces

We next investigated whether GFP^{HI} cells exhibited an attenuated response at more proximal events of T cell activation upon stimulation with cognate peptide. Among the early T cell responses to

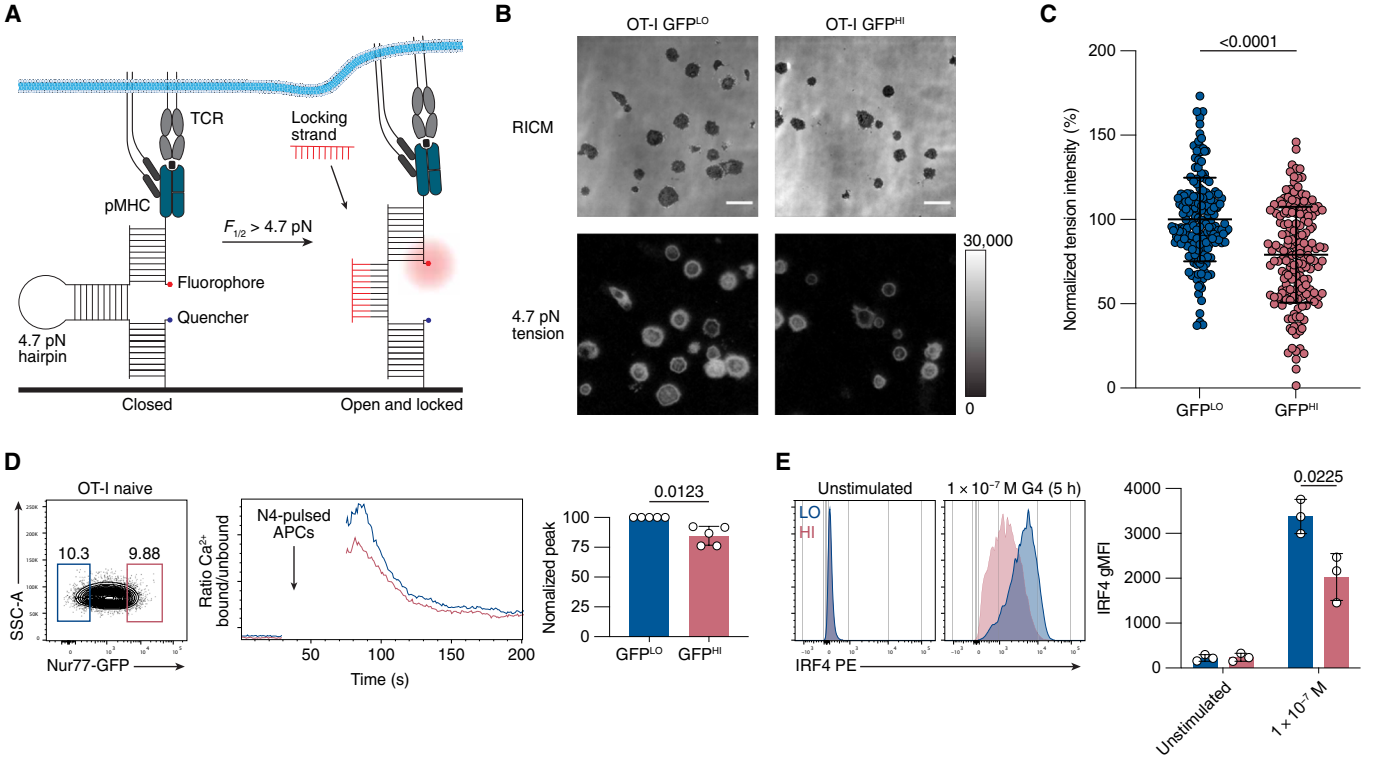

Fig. 4. Nur77-GFP^{HI} CD8$^+$ T cells exert less TCR-mediated tension forces and exhibit attenuated proximal and integrated TCR signaling. (**A**) Schematic outline of the DNA hairpin–based tension probe. In its closed conformation, the fluorescence of Atto647N is quenched. The DNA hairpin unfolds when TCR-mediated tension exceeds 4.7 pN. A "locking" DNA strand that hybridizes to the mechanically unfolded probe stabilizes the unfolded conformation of the DNA hairpin. (**B**) Representative reflection interference contrast microscopy (RICM) and fluorescence images showing GFP^{LO} and GFP^{HI} OT-I CD8$^+$ T cells spread on DNA hairpin tension probe–coated surfaces after 30 min. Scale bars, 10 μm. (**C**) Graph displays the normalized unquenched fluorescence intensities of the unfolded tension probes for 176 to 180 cells from three independent experiments (each symbol represents one cell). (**D**) Baseline Ca^{2+} levels were recorded for 30 s, and the arrow indicates the time point when the T cells were mixed with N4-pulsed APCs, centrifuged, and resuspended before the continuation of data acquisition. Contour plot shows the distribution of Nur77-GFP fluorescence intensity for CD8$^+$ CD44^{LO} OT-I T cells. Numbers indicate the percentages of cells within the indicated gates, representing GFP^{LO} and GFP^{HI} cells (left). Histogram shows the mean values for the relative concentration of free Ca^{2+} over time in GFP^{LO} and GFP^{HI} naive OT-I CD8$^+$ T cells (middle). The bar graph shows the normalized peak intracellular free Ca^{2+} values during 10 s of GFP^{LO} and GFP^{HI} cells ~70 s after the initial acquisition (right). (**E**) Histograms depict the IRF4 staining intensity of FACS-sorted GFP^{LO} and GFP^{HI} OT-I cells that were either unstimulated (left) or stimulated for 5 hours with 1×10^{-7} M G4 peptide and APCs. Bar graph displays the IRF4 gMFI. Data in (B), (C), and (E) represent three independent experiments with $n = 3$ mice or biological replicates. Data in (D) represent three independent experiments with $n = 5$ mice. In (C) to (E), bars depict means and error bars show ±SD. Statistical testing was performed by unpaired two-tailed Student's *t* test in (C) and (E) or unpaired two-tailed Student's *t* test with Welch's correction (D).

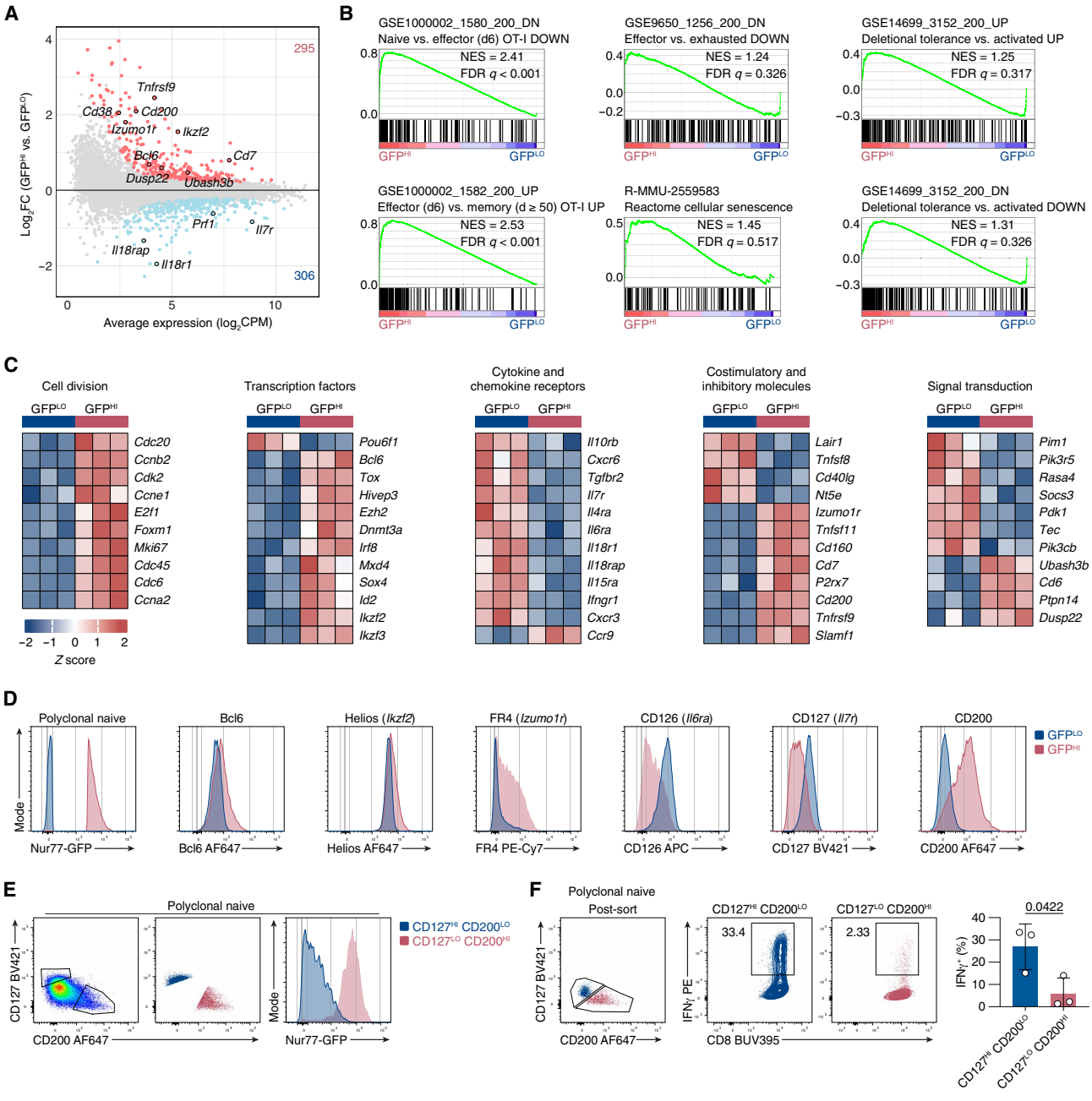

Fig. 5. Nur77-GFP expression in naive CD8$^+$ T cells during steady-state conditions correlates with gene expression changes. (**A**) MA plot of DEGs between GFP^{LO} and GFP^{HI} naive OT-I CD8$^+$ T cells. DEGs were defined as genes with FDR < 0.05. Selected genes have been highlighted. The number of differentially expressed genes in GFP^{HI} relative to GFP^{LO} cells is indicated in red and blue, respectively. (**B**) GSEA of genes with decreased expression in naive compared with effector CD8$^+$ T cells (top left) and more highly expressed genes in effector compared with resting memory CD8$^+$ T cells (bottom left) (*51*). GSEA of genes with decreased expression in effector compared with exhausted CD8$^+$ T cells (top middle) and genes associated with cellular senescence (bottom middle) (*107*). GSEA of more highly expressed genes (top right) or genes with decreased expression (bottom right) in cells subjected to deletional tolerance compared with activated CD8$^+$ T cells (*108*). FDR values were derived from running GSEA on the c7_Immunesigdb.v2022.1 database or the c2.cp.reactome.v2023.1 database. (**C**) Curated heatmaps of normalized expression of DEGs in indicated categories. (**D**) Histograms show the expression of the indicated markers by GFP^{LO} and GFP^{HI} cells. The cells were gated on naive, polyclonal CD8$^+$ T cells. Bar graphs depict gMFI of indicated proteins. (**E**) Flow cytometry plots (left, middle) show the gating scheme to identify CD127^{HI} CD200^{LO} and CD127^{LO} CD200^{HI} populations. Histogram (right) shows the GFP fluorescence intensity for CD127^{HI} CD200^{LO} and CD127^{LO} CD200^{HI} populations. Plots depict naive, polyclonal Nur77-GFP CD8$^+$ T cells. (**F**) Cells were stimulated for 24 hours with anti-CD3 (0.25 μg/ml) and APCs before an IFN-γ secretion assay was performed. Overlaid dot plot of sorted CD127^{HI} CD200^{LO} and CD127^{LO} CD200^{HI} naive polyclonal CD8$^+$ T cells (left). Contour plots (middle and right) depict CD8 and IFN-γ expression by stimulated viable polyclonal CD8$^+$ T cells after a 45-min IFN-γ secretion assay. Numbers indicate the percentage of cells within the indicated gates. Bar graph displays the frequencies of CD127^{HI} CD200^{LO} and CD127^{LO} CD200^{HI} IFN-γ–secreting cells. Bars depict the mean, error bars show ±SD, and each symbol represents one mouse. Statistical testing was performed by unpaired two-tailed Student's *t* test. Data in (D) to (F) represent two or three independent experiments with $n = 3$ to 6 mice. NES, normalized enrichment score.

pMHC stimulation is the exertion of mechanical forces through the TCR (*46*), which positively correlates with increases in the intensity of ZAP-70 phosphorylation, suggesting a positive regulatory role for mechanical forces in early T cell activation (*47*). To test our hypothesis that GFP^{LO} and GFP^{HI} cells would exhibit differences in tension exerted on pMHC ligands, we used DNA hairpin–based "tension" probes linked to pMHC. The tension probe consists of a DNA hairpin conjugated to fluorophore (Atto647N) and quencher (BHQ2) molecules positioned to quench fluorescence by fluorescence resonance energy transfer (FRET) when the DNA hairpin is in its closed configuration (Fig. 4A) (*48*). When a T cell applies forces to a pMHC molecule through its TCR with a magnitude exceeding 4.7 pN, the DNA hairpin unfolds, separating the FRET pair and causing dequenching of the dye. A "locking" DNA strand is then introduced to selectively hybridize to the mechanically unfolded DNA hairpin and prevent refolding to capture the tension signal. After isolating GFP^{LO} and GFP^{HI} OT-I cells, we cultured them on substrates coated with tension probes conjugated to H2-K^b loaded with OVA N4 peptide (fig. S4, A and B). On average, GFP^{LO} cells induced a 20% higher fluorescence signal from the tension probes than did GFP^{HI} cells (Fig. 4, B and C). These results indicate that GFP^{LO} cells were more likely to exert the 4.7-pN tension force required to unfold the DNA hairpins than GFP^{HI} cells in response to pMHC stimulation.

We next sought to determine whether GFP^{LO} and GFP^{HI} naive $CD8^+$ T cells exhibited differences in proximal TCR signaling. We hypothesized that naive GFP^{HI} OT-I T cells would exhibit decreased cytosolic Ca^{2+} concentrations relative to GFP^{LO} cells upon stimulation with cognate N4 peptide antigen. We used flow cytometry to analyze OT-I cells labeled with the Ca^{2+} ratiometric indicator dye Indo-1 and coincubated with N4 peptide-pulsed APCs. Compared with the peak free Ca^{2+} concentration signal generated by GFP^{LO} cells, the peak signal generated by GFP^{HI} cells was reduced by 20% (Fig. 4D). Together, these data suggest that GFP^{HI} naive $CD8^+$ T cells, which previously experienced more TCR signaling in the basal state, trigger downstream signals with weaker intensity in response to subsequent TCR stimulation. These results are consistent with a previous study using CD5 as a surrogate marker of self-pMHC reactivity, which showed an inverse correlation between the intensity of CD5 expression and the magnitude of anti-CD3–induced Ca^{2+} increases in naive $CD8^+$ T cells (*23*).

We further hypothesized that naive GFP^{HI} OT-I cells would exhibit attenuated integrated TCR signaling in response to antigen stimulation. Increased expression of the transcription factor interferon regulatory factor 4 (IRF4) occurs within hours of TCR stimulation and is sensitive to both antigen affinity and antigen dose in $CD8^+$ T cells (*49*, *50*). Hence, we sorted naive GFP^{LO} and GFP^{HI} OT-I cells to investigate the induced IRF4 expression 5 hours after stimulation with the weak agonist peptide G4. On average, the gMFI of IRF4 staining intensity in GFP^{LO} cells was 1.6-fold higher than in GFP^{HI} cells (Fig. 4E). Thus, naive GFP^{HI} cells exhibit a reduced intensity of integrated TCR signaling within hours of stimulation compared with GFP^{LO} cells.

Extensive tonic TCR signaling in naive $CD8^+$ T cells correlates with differences in gene expression

To identify gene expression patterns associated with increased tonic TCR signaling in naive $CD8^+$ T cells, we performed RNA-sequencing (RNA-seq) analysis of GFP^{LO} and GFP^{HI} naive $CD8^+$ $CD44^{LO}$ $CD62L^{HI}$ $Qa2^{HI}$ OT-I cells. We detected a total of 601 differentially expressed genes (DEGs) at a false discovery rate (FDR) of <0.05 (Fig. 5A). Considering the correlation between Nur77-GFP expression and TCR signal strength, we hypothesized that GFP^{HI} cells would exhibit a gene expression profile with more similarities to acutely stimulated cells than GFP^{LO} cells. Comparison of our dataset with DEGs that are more highly expressed in effector OT-I cells compared with naive cells (*51*) by gene set enrichment analysis (GSEA) revealed that GFP^{HI} cells showed an enrichment of genes more highly expressed in effector $CD8^+$ T cells (Fig. 5B).

In addition, we compared the degree of overlap between DEGs in naive GFP^{HI} and GFP^{LO} cells and between DEGs in *Listeria* infection–induced OT-I effector cells and naive OT-I cells (fig. S5A) (*52*). We detected a significant positive correlation between genes enriched in GFP^{HI} cells and acutely stimulated OT-I cells (fig. S5B). These results suggested that the effects of extensive tonic TCR signaling share similarities with the gene expression changes associated with acutely stimulated and effector $CD8^+$ T cells. However, GFP^{HI} cells also showed enrichment of genes more highly expressed in effector OT-I cells compared with resting memory cells (Fig. 5B). We did not detect a statistically significant enrichment of genes associated with T cell exhaustion, senescence, or deletional tolerance in GFP^{HI} cells (Fig. 5B). We next sought to explore DEGs in GFP^{HI} naive $CD4^+$ and $CD8^+$ T cells. The overlapping DEGs between GFP^{LO} and GFP^{HI} naive $CD8^+$ T cells and the DEGs more highly expressed in naive GFP^{HI} $Ly6C^-$ $CD4^+$ T cells (fig. S5C) (*7*) positively correlated (fig. S5D). Hence, extensive tonic TCR signals induced similar transcriptional changes in naive $CD4^+$ and $CD8^+$ T cells.

In addition, we detected increased transcripts of genes involved in cell division in GFP^{HI} relative to GFP^{LO} cells, consistent with a gene signature indicative of acutely activated T cells (Fig. 5C). In agreement, naive $CD8^+$ T cells that experience stronger tonic TCR signals and express higher levels of CD5 likewise show enrichment for cell cycle–associated genes (*53*). GFP^{HI} cells also expressed higher levels of transcription factors associated with T cell differentiation, such as *Bcl6* and *Ikzf2* (which encodes Helios), and TCR stimulation, such as *Tox* and *Irf8* (Fig. 5C) (*54*–*56*). Consistent with a gene signature of T cell activation, GFP^{HI} cells increased expression of immunomodulatory molecules such as *Tnfrsf9* (which encodes 4-1bb), *Tnfsf11* (which encodes Rankl), and *Cd200* (Fig. 5C) (*57*–*60*). GFP^{HI} cells expressed lower levels of *Il7r* (which encodes CD127) in addition to other common γ-chain cytokine receptors such as *Il4ra*, *Il6ra* (which encodes CD126), and *Il15ra* (Fig. 5C). Among genes involved in signal transduction, GFP^{HI} cells had lower expression of genes encoding kinases such as Pim1 and Pdk1. In contrast, GFP^{HI} cells expressed higher levels of *Ubash3b* (which encodes Sts1), *Dusp22* (which encodes Jkap), and *Ptpn14*, all of which encode phosphatases (Fig. 5C). Together, gene expression patterns associated with higher levels of tonic TCR signaling bore similarities to gene expression patterns induced by acute TCR stimulation. This gene signature included higher expression levels of immunomodulatory receptors and ligands, including negative regulators of TCR signaling.

We next performed flow cytometry analyses to determine whether differential gene expression patterns correlated with differential protein expression. We compared the protein levels of several DEGs in naive, polyclonal $CD8^+$ GFP^{LO} and GFP^{HI} T cells. These DEGs included *Bcl6*, *Ikzf2* (Helios), *Izumo1r* (folate receptor 4), *Il6ra* (CD126), *Il7ra* (CD127), and *Cd200* (Fig. 5D and fig. S5E). For

four of the six selected DEGs, protein staining was increased in GFP^{HI} relative to GFP^{LO} cells and thus correlated with the RNA-seq data. GFP^{HI} cells expressed lower surface levels of CD126 and CD127, consistent with the RNA-seq analysis. Flow cytometry analysis of naive CD8^{+} T cells showed a range of CD127 and CD200 expression (Fig. 5E). Within the naive CD8^{+} population, the CD127^{HI} CD200^{LO} cell subset enriched for Nur77-GFP^{LO} cells and, in contrast, the CD127^{LO} CD200^{HI} population enriched for GFP^{HI} cells (Fig. 5E). Thus, Nur77-GFP^{LO} and Nur77-GFP^{HI} cells exhibit differential mRNA and protein expression.

We hypothesized that CD127^{LO} CD200^{HI} cells would exhibit an attenuated responsiveness similar to that of GFP^{HI} cells. To test this hypothesis, we performed an IFN-γ secretion assay with CD127^{HI} CD200^{LO} (GFP^{LO}-like) and CD127^{LO} CD200^{HI} (GFP^{HI}-like) naive CD8^{+} T cells sorted from WT mice and stimulated with APCs and anti-CD3 antibodies (Fig. 5F and fig. S5F). On average, the frequency of IFN-γ–secreting CD127^{LO} CD200^{HI} (GFP^{HI}-like) cells was more than fourfold lower than the frequency of IFN-γ–secreting CD127^{HI} CD200^{LO} (GFP^{LO}-like) cells (Fig. 5F). These results suggest that GFP^{HI}-like naive CD8^{+} T cells from WT mice exhibit

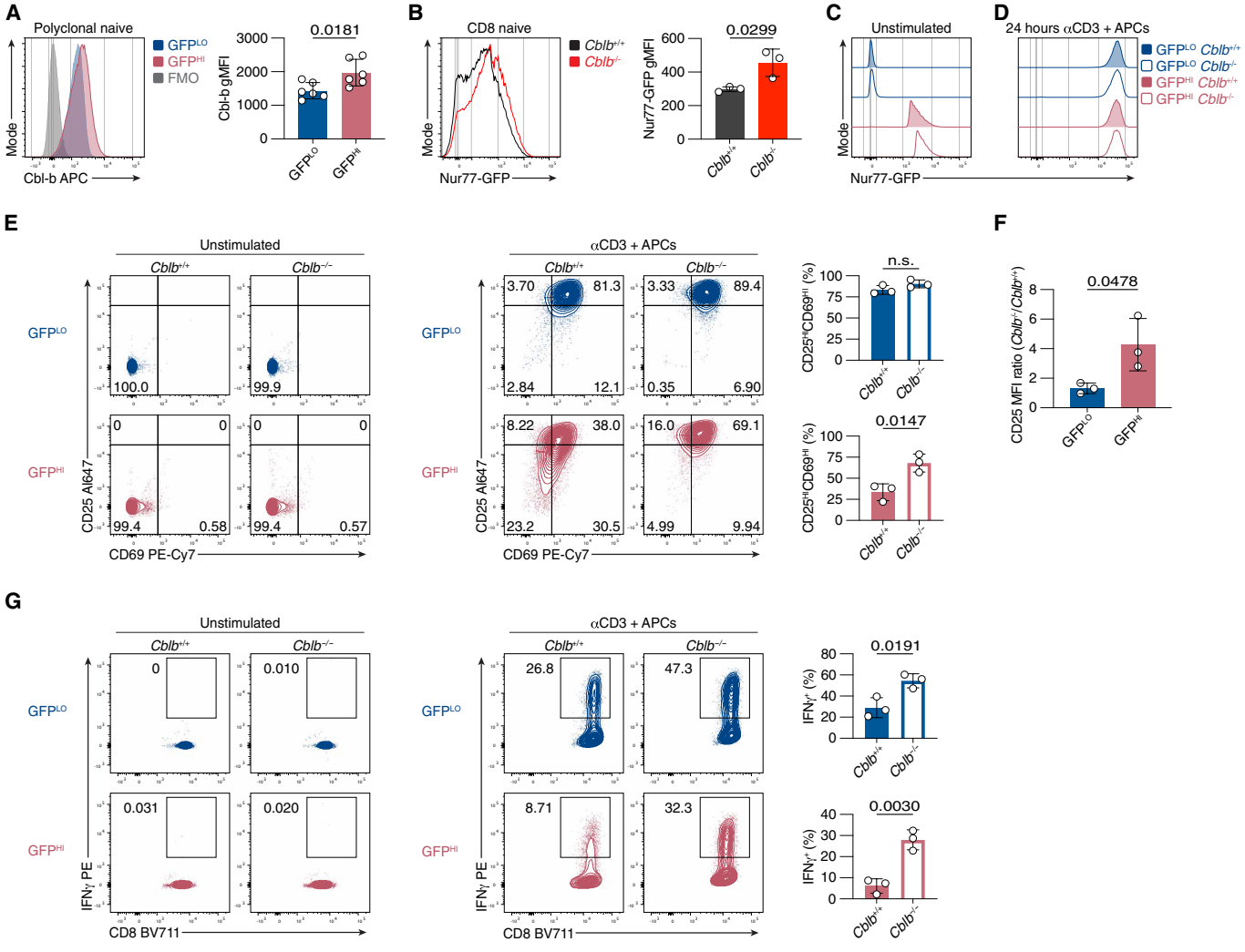

Fig. 6. Increased Cbl-b abundance in naive GFP^{HI} cells contributes to the attenuation in responsiveness. (**A**) Histogram depicts the staining intensity of Cbl-b in naive polyclonal GFP^{LO} and GFP^{HI} CD8^{+} T cells. Bar graph displays the Cbl-b gMFI from three independent experiments. (**B**) Histogram depicts the Nur77-GFP fluorescence intensity of naive polyclonal CD8^{+} T cells from *Cbl-b*$^{+/+}$ (black) and *Cbl-b*$^{-/-}$ (red) mice. Bar graph shows Nur77-GFP gMFI values. (**C** and **D**) Histograms display Nur77-GFP expression in naive polyclonal GFP^{LO} (blue) and GFP^{HI} (red) cells from *Cbl-b*$^{+/+}$ (filled symbols) or *Cbl-b*$^{-/-}$ (open symbols) mice. Cells were either unstimulated (left) or stimulated for 24 hours with anti-CD3 (0.25 μg/ml) and APCs (right). (**E**) Contour plots depict CD25 and CD69 expression in naive, polyclonal GFP^{LO} and GFP^{HI} CD8^{+} T cells that were either unstimulated (left) or stimulated as in (D) (right). Numbers indicate the percentage of cells within the indicated gates. Bar graphs show the percentages of CD25^{HI} CD69^{HI} cells. (**F**) Bar graph depicts the ratio of the CD25 MFI of *Cbl-b*$^{-/-}$ to *Cbl-b*$^{+/+}$ mice. (**G**) Contour plots of IFN-γ secretion from CD8^{+} T cells that were either unstimulated (left) or stimulated as in (D), after a 45-min IFN-γ secretion assay (right). Numbers indicate the percentage of cells within the indicated gates. Bar graphs show the percentages of IFN-γ^{+} cells. Data in (A) represent three independent experiments with $n = 6$ mice. Data in (B) to (G) represent three independent experiments with $n = 3$ mice or biological replicates. In (A), (B), and (E) to (G), bars depict means, error bars depict ±SD, and each symbol represents one mouse or biological replicate. Statistical testing was performed by unpaired two-tailed Student's *t* test. FMO, fluorescence minus one control.

attenuated early responsiveness and a similar functional phenotype as Nur77-GFP^{HI} naive CD8$^+$ T cells.

Cbl-b deficiency partially rescues the responsiveness of GFP^{HI} naive CD8$^+$ T cells

We hypothesized that increased expression of negative regulators mitigates the activation of GFP^{HI} cells. We previously showed that naive GFP^{HI} Ly6C$^-$ CD4$^+$ T cells express higher protein levels of the E3 ubiquitin ligase Cbl-b, a negative regulator of TCR signaling (*18*, *61*). We hypothesized that similarly to their CD4$^+$ counterparts, CD8$^+$ GFP^{HI} cells would express higher levels of Cbl-b. Our RNA-seq analyses did not detect a significant difference in *Cblb* mRNA levels between GFP^{LO} and GFP^{HI} naive CD8$^+$ T cells. We next compared Cbl-b protein expression by GFP^{LO} and GFP^{HI} cells by intracellular staining. The gMFI of Cbl-b staining intensity in GFP^{HI} cells was almost 1.5-fold higher than in GFP^{LO} cells (Fig. 6A). Hence, extensive tonic TCR signaling was associated with increased Cbl-b protein levels in naive CD8$^+$ T cells.

Considering the inhibitory function of Cbl-b in the TCR signal transduction pathway and its increased expression in GFP^{HI} cells, we hypothesized that Cbl-b deficiency would rescue the attenuated responsiveness of GFP^{HI} cells. To test this hypothesis, we generated *Cblb*$^{-/-}$ Nur77-GFP mice. Naive *Cblb*$^{+/+}$ and *Cblb*$^{-/-}$ CD8$^+$ cells expressed Nur77-GFP, although the gMFI of GFP was higher in *Cblb*$^{-/-}$ cells (Fig. 6B). We next sorted for GFP^{LO} and GFP^{HI} naive CD8$^+$ cells from *Cblb*$^{+/+}$ and *Cblb*$^{-/-}$ Nur77-GFP mice (Fig. 6C). After stimulation for 24 hours with APCs and anti-CD3 antibodies, Nur77-GFP fluorescence intensities were similar in *Cblb*$^{+/+}$ and *Cblb*$^{-/-}$ cells (Fig. 6D). The frequency of GFP^{HI} cells that increased expression of CD25 and CD69 after 24 hours of stimulation was approximately twofold higher in *Cblb*$^{-/-}$ compared with *Cblb*$^{+/+}$ cells (Fig. 6E). The frequencies of CD25^{HI}CD69^{HI} cells were higher in GFP^{LO} cells and not significantly different between *Cblb*$^{+/+}$ and *Cblb*$^{-/-}$ cells (Fig. 6E). In a complementary approach, we analyzed Cbl-b–deficient naive CD8$^+$ T cells using the CD127^{HI} CD200^{LO} (GFP^{LO}-like) and CD127^{LO} CD200^{HI} (GFP^{HI}-like) gating strategy (fig. S6, A and B). Whereas the frequency of CD25^{HI}CD69^{HI} cells was more than 10-fold higher in *Cblb*$^{-/-}$ relative to *Cblb*$^{+/+}$ GFP^{HI}-like cells, the proportion of CD25^{HI}CD69^{HI} cells was 1.5-fold higher in *Cblb*$^{-/-}$ compared with *Cblb*$^{+/+}$ GFP^{LO}-like cells (fig. S6C).

We next quantified the increases in CD25 gMFI in *Cblb*$^{+/+}$ and *Cblb*$^{-/-}$ populations. The CD25 gMFI increased for both GFP^{LO} and GFP^{HI} populations after stimulation. However, the fold increase in CD25 gMFI was about threefold higher for GFP^{HI} than GFP^{LO} cells (Fig. 6F). We next compared the CD25 gMFI between *Cblb*$^{-/-}$ and *Cblb*$^{+/+}$ GFP^{LO}-like and GFP^{HI}-like cells. The CD25 gMFI increased in both populations of *Cblb*$^{-/-}$ cells (fig. S6D). These data suggest that the CD25 expression by GFP^{HI} cells was rescued to a greater extent by Cbl-b deficiency than in GFP^{LO} cells.

We next asked how Cbl-b deficiency affected the secretion of IFN-γ in GFP^{LO} and GFP^{HI} cells. After 24 hours of stimulation with anti-CD3 and splenocyte APCs, we performed an IFN-γ capture assay. The frequency of *Cblb*$^{-/-}$ GFP^{HI} cells that secreted IFN-γ was about 4.6-fold higher compared with *Cblb*$^{+/+}$ GFP^{HI} cells (Fig. 6G). Among GFP^{LO} cells, Cbl-b deficiency increased the frequency of IFN-γ–secreting cells almost twofold (Fig. 6G). We next asked whether Cbl-b deficiency could also rescue the secretion of IFN-γ in GFP^{HI}-like cells. The frequency of IFN-γ–secreting cells was more than 30-fold higher in *Cblb*$^{-/-}$ GFP^{HI}-like cells relative to *Cblb*$^{+/+}$ GFP^{HI}-like cells (fig. S6E). IFN-γ secretion was more than fourfold higher in GFP^{LO}-like Cbl-b–deficient T cells compared with GFP^{LO}-like *Cblb*$^{+/+}$ cells (fig. S6E). Together, these results indicate that naive GFP^{LO} and GFP^{HI} CD8$^+$ T cells differentially expressed Cbl-b at the protein level and were more responsive to TCR stimulation in the absence of Cbl-b. However, some GFP^{HI} responses, such as increased CD25 expression, were rescued to a greater extent by Cbl-b deficiency. These data support a model where extensive tonic TCR signals induce negative regulation, partly mediated by increased Cbl-b expression.

DISCUSSION

In this study, we found that the intensity of Nur77-GFP reporter transgene expression by naive CD8$^+$ T cells inversely correlated with their responsiveness to TCR stimulation. Hence, we propose a model in which extensive tonic TCR signaling induces negative feedback mechanisms that limit the responsiveness to subsequent TCR stimulations. Naive T cells express the Nur77-GFP reporter transgene in a manner that is influenced by the strength, frequency, and recency of tonic TCR signals. Our findings showed that Nur77-GFP expression in naive CD8$^+$ T cells depended on continuous exposure to β2m/MHC I, indicating that recurrent TCR signals continuously drive Nur77-GFP expression. These results are consistent with a previous study that showed that naive T cells engage in multiple transient interactions with APCs that last for less than 5 min per interaction, on average (*62*). These findings suggest that naive T cells experience discontinuous tonic TCR signaling during these short-lived interactions with APCs. The GFP proteins expressed as a result of TCR stimulation persist in T cells with a half-life of 26 to 54 hours, longer than most T cell:APC interactions (*32*, *33*). In light of these results, we conclude that Nur77-GFP expression in naive T cells can reflect cumulative tonic TCR signals experienced by T cells as they scan APCs in SLOs. On the other hand, it is formally possible that expression of relatively high levels of Nur77-GFP in naive T cells reflects recent acute TCR stimulation. However, studies of the reporter transgene Nur77-Tempo suggest that this may not be the case. In Nur77-Tempo transgenic mice, the *Nr4a1* promoter drives the expression of a fluorescent timer (FT) protein (*63*), which undergoes a shift in its fluorescence emission spectrum with a half-life of around 4 hours in T cells (*64*). CD69$^-$ CD8$^+$ T cells in the spleen show nondetectable levels of the less mature form of FT, indicating that FT expression in naive T cells is likely not driven by recent strong TCR signaling. These results are consistent with a model in which fluorescent reporters can reflect the accumulated output of multiple discontinuous tonic TCR signals experienced by naive T cells. Considering these findings and the decay of Nur77-GFP in naive CD8$^+$ T cells seen after 10 days in *B2m*$^{-/-}$ mice, we interpret steady-state Nur77-GFP expression in naive T cells to reflect the accumulation of TCR signaling events occurring within days.

The influence of discrete, recurrent TCR signaling events on T cell biology is also apparent during development. For example, CD4$^+$ CD8$^+$ double-positive thymocytes experience multiple transient TCR stimulations over hours to days during thymic positive selection, as observed by transient Ca^{2+} increases (*65*). Inhibition of ZAP-70 kinase activity decreases the intensity and frequency of these discontinuous signaling events and correlates with an impairment in positive selection (*66*).

Our gene expression analyses revealed similarities in the gene expression profiles of naive GFP^{HI} T cells and activated T cells. One similar feature is differential expression of genes that encode for proteins that can inhibit TCR-induced signal transduction. This finding is reminiscent of a study showing that constitutive agonist TCR stimulation in mice unperturbed by infection or inflammatory mediators is associated with tolerogenic responses in CD4$^+$ T cells (*67*). In this system, constitutive expression of even low doses of cognate antigen over an extended period induces increased expression of genes associated with anergy (*67*). Furthermore, we previously found a gene expression profile associated with T cell activation and negative regulation in naturally occurring naive Nur77-GFP^{HI} CD4$^+$ T cells (*7*). Moreover, naive CD4$^+$ T cells expressing a hyperactive ZAP-70 mutant show increased tonic TCR signaling but reduced responsiveness to agonist TCR stimulation, the latter of which was restored by Cbl-b deficiency (*68*). These studies suggest that extensive TCR signals can induce negative feedback mechanisms.

Nur77-GFP expression in naive CD8$^+$ T cells positively correlated with increased protein levels of the ubiquitin ligase Cbl-b. Here, we propose that the attenuated responsiveness of the most self-reactive naive CD8$^+$ T cells due to induced negative regulation depends at least partially on the ubiquitin ligase Cbl-b. Cbl-b is a negative regulator of T cell activation (*61*), and Cbl-b–deficient T cells exhibit many altered signal transduction pathways in response to TCR signaling, such as increased nuclear factor κB (NF-κB) activation and Vav1 phosphorylation (*69*, *70*).The signalosome of Cbl-b in CD4$^+$ T cells consists of nearly 100 interacting partners, including the phosphatases Sts1 and Sts2 (*71*). Thus, Cbl-b may facilitate recruitment of Sts1 and Sts2 to the TCR complex, where they may inhibit signal transduction through dephosphorylation of tyrosine kinases such as ZAP-70 (*72*).

The Nr4a family transcription factors restrain peripheral T cell responses (*73*). Consistent with this concept, in vivo–tolerized murine T cells express high levels of *Nr4a1*, and *Nr4a1* overexpression results in increased expression of anergy-associated genes, including *Cblb* (*74*). *Nr4a1* deficiency results in resistance to anergy induction and increased autoimmune disease severity (*74*–*76*). Moreover, *Nr4a1*$^{-/-}$ *Nr4a2*$^{-/-}$ *Nr4a3*$^{-/-}$ chimeric antigen receptor (CAR) T cells show enhanced antitumor responses in a solid tumor mouse model (*77*). These studies suggest that *Nr4a1* and the other *Nr4a* family genes can act as negative regulators (*78*). We propose that the increased expression of *Nr4a1* in Nur77-GFP^{HI} naive CD8$^+$ cells is part of a negative feedback mechanism also associated with strong tonic TCR stimulation.

Our differential gene expression analyses suggested that strong tonic TCR signaling increased the expression of genes associated with acute TCR stimulation, as well as those encoding phosphatases *Ubash3b* (which encodes Sts1), *Dusp22* (which encodes Jkap), and *Ptpn14*, which can inhibit intracellular signaling in naive OT-I GFP^{HI} cells. *Ubash3b*$^{-/-}$ and *Ubash3b*$^{-/-}$ *Ubash3a*$^{-/-}$ T cells are hyperresponsive to TCR stimulation (*72*, *79*). Sts1's role in inhibiting T cell responsiveness may involve inhibiting ZAP-70 through the dephosphorylation of regulatory tyrosine residues (*72*). The phosphatase Jkap can dephosphorylate kinases of the proximal TCR signaling cascade, whereas Ptpn14 has unclear functions in T cells (*80*, *81*). The increased expression of genes encoding these phosphatases in GFP^{HI} cells is consistent with the increased expression of the phosphatase Ptpn2 in CD5^{HI} over CD5^{LO} naive CD8$^+$ T cells (*82*). Furthermore, T cells deficient in *Ptpn2* tend to undergo more extensive lymphopenia-induced proliferation, suggesting that Ptpn2 negatively inhibits TCR:self-pMHC signaling (*82*).

CD5-deficient T cells are hyperresponsive to TCR stimulation, suggesting that CD5 can act as a negative regulator of TCR signaling (*83*, *84*). CD5 and Nur77-GFP are both surrogate markers of tonic TCR signaling (*3*). However, although CD5 staining intensity positively correlates with Nur77-GFP expression in naive CD8$^+$ T cells, we showed in this study that GFP^{LO} and GFP^{HI} cells still have overlapping CD5 staining intensity. Likewise, CD5^{LO} and CD5^{HI} naive CD8$^+$ T cells have overlapping Nur77-GFP expression (*27*). Hence, CD5^{HI} and Nur77-GFP^{HI} expression phenotypes mark different cell populations. Similarly, CD5^{LO} and Nur77-GFP^{LO} expression phenotypes label diverging cell populations. We propose that the differences in cellular compositions of CD5^{LO} and GFP^{LO} (or CD5^{HI} and GFP^{HI}) cell populations can lead to different functional phenotypes. For example, CD5^{HI} naive CD8$^+$ T cells have a competitive advantage over CD5^{LO} cells in response to foreign antigen stimulation (*27*, *85*). In contrast, our results suggest that GFP^{LO} cells have a competitive advantage over GFP^{HI} cells. Understanding the differences between CD5 and *Nr4a1* reporter expression as markers of tonic TCR signaling would require additional studies.

The increased expression of negative regulators in naive T cells in response to tonic TCR signaling is consistent with models proposing that T cell responsiveness depends on previously experienced TCR signals (*9*, *86*). A negative feedback loop is one way in which relatively strong basal TCR signaling could effectively result in T cell desensitization and hyporesponsiveness to subsequent TCR stimulations. "Adaptive tuning" in this context could attenuate the responsiveness of the naive T cells that respond most intensely to self-pMHC (*87*). Strong TCR stimulation of naive T cells can recalibrate the activation thresholds of recently stimulated T cells through increased expression of checkpoint receptor expression (*88*).

Variable levels of Nur77-GFP expression appear to correlate with functional heterogeneity within the naive CD8$^+$ T cell population. Tonic TCR signal strength may influence such variations at the single-cell level. Lineage-tracing studies have previously identified diversity in the expansion and differentiation of single TCR-transgenic T cells through primary and recall responses (*89*). Cellular heterogeneity may also contribute to the dynamic nature of adaptive immune responses to respond to a breadth of antigens (*11*, *90*). In conclusion, we observed reduced responsiveness in GFP^{HI} naive CD8$^+$ T cells that have experienced extensive tonic TCR stimulation. We speculate that such negative feedback mechanisms may constitute a form of cell-intrinsic tolerance in naive T cells.

MATERIALS AND METHODS

Mice

Nur77-GFP [Tg(Nr4a1-EGFP)GY139Gsat] transgenic mice, ZAP-70–deficient mice lacking mature T cells (Zap70tm1Weis), and Foxp3-RFP (red fluorescent protein) mice (C57BL/6-Foxp3tm1Flv/J) have been previously described (*14*, *91*, *92*). C57BL/6J mice (WT mice in the text), CD45.1 mice (B6.SJL-Ptprca Pepcb/BoyJ), and *B2m*$^{-/-}$ mice (B6.129P2-B2mtm1Unc/DcrJ) were purchased from the Jackson Laboratory (*93*). Where noted, the Nur77-GFP strain was interbred with the CD45.1 strain. A Nur77-GFP strain that is interbred with the OT-I [C57BL/6-Tg(TcraTcrb)1100Mjb/J] TCR-transgenic strain was described previously (*15*). This OT-I-Nur77-GFP strain was interbred with a

Trac$^{-/-}$ strain (B6.129S2-Tcratm1Mom/J) purchased from the Jackson Laboratory. A Nur77-GFP strain interbred with the Foxp3-RFP strain has previously been described (*18*). P14 mice have been described before and were provided by R. Ahmed at Emory University (*94*). P14 mice on the C57BL/6J background were interbred with the Nur77-GFP and CD45.1 strains. All mice were housed under specific pathogen–free conditions in the Division of Animal Resources at Emory University. The *Cblb*$^{-/-}$ strain was previously described and was interbred with the Nur77-GFP strain (*95*). These two strains were maintained in the Laboratory Animal Resource Center at the University of California, San Francisco. Both female and male mice were used throughout the study. All animal experiments were conducted in compliance with the Institutional Animal Care and Use Committees at Emory University (PROTO201700761) and the University of California, San Francisco (AN184320-02D).

Antibodies and reagents

The antibodies and reagents used in this study are listed in table S1. For the negative enrichment of CD8$^+$ T cells, the following biotinylated anti-mouse or anti-mouse/human antibodies were used: CD4 (clone RM4-5), CD19 (6D5), B220 (RA3-6B2), CD11b (M1/70), CD11c (N418), CD49b (DX5), and erythroid cells (TER119). For the negative selection of APCs, biotinylated anti-CD4 (RM4-5), anti-CD8α (53-6.7), and anti-erythroid cells (TER119) were used.

Lymphocyte isolation and flow cytometry

Single-cell suspensions of lymphoid organs were generated by mashing organs through a 70-μm cell strainer or using a Dounce homogenizer. For phenotypic analysis of T cells by flow cytometry, RBCs were lysed using RBC Lysis Buffer (Tonbo Biosciences) before Fc-block incubation (anti-mouse CD16/CD32, clone 2.4G2). CD8$^+$ T cells were purified by negative selection using biotinylated antibodies and magnetic beads as previously described (*96*). Splenocytes were used as APCs, isolated from *Zap70*$^{-/-}$ or *Trac*$^{-/-}$ mice after RBC lysis or by negative selection using biotinylated antibodies and magnetic beads on single-cell suspensions from C57BL/6 mice. Single-cell suspensions were stained in phosphate-buffered saline (PBS) and washed with fluorescence-activated cell sorting (FACS) buffer [PBS with 0.5% bovine serum albumin (BSA) and 2 mM EDTA] for surface stains. For intracellular Bcl6, Helios, and IRF4 staining, samples were fixed and permeabilized with the Foxp3/Transcription Factor Staining kit (Thermo Fisher Scientific) according to the manufacturer's instructions. For intracellular staining of TCR-β and Cbl-b, samples were fixed with 4% paraformaldehyde in PBS and permeabilized with Perm/Wash buffer (BD Biosciences) according to the manufacturer's instructions. Intracellular staining was performed at room temperature. Cbl-b was stained with a primary rabbit anti-mouse antibody and a secondary stain with a donkey anti-rabbit immunoglobulin G FAB fragment (Jackson ImmunoResearch). For in vitro proliferation analysis, T cells were labeled with CellTrace Violet (Thermo Fisher Scientific) according to the manufacturer's instructions. Samples were analyzed using FACSymphony A5 (BD Biosciences), FACSymphony A3 (BD Biosciences), LSRFortessa (BD Biosciences), or Cytek Aurora instruments. Flow cytometry data were analyzed using FlowJo v.10.8.1 software (BD Biosciences).

Intravascular labeling

Intravascular labeling was performed as previously described (*97*). Briefly, 3 μg of anti-CD45.2-allophycocyanin antibody was injected in 200 μl of PBS intravenously 3 min before euthanasia. Cells from the spleen were analyzed by flow cytometry. Lymph nodes and peripheral blood were harvested as negative and positive controls, respectively. Positive CD45 staining was interpreted as the cells being located within the red pulp; the absence of CD45 staining was interpreted as the cells being located within the white pulp.

Cell sorting

Naive CD8$^+$ GFP^{LO} and GFP^{HI} T cells were sorted from bulk CD8$^+$ T cells using a FACSAria II SORP cell sorter (BD Bioscience). TCR polyclonal naive T cells were sorted on the basis of the following cell surface phenotype: CD8$^+$ CD44^{LO} CD62L^{HI} and excluding a viability dye. Naive OT-I cells were sorted on the basis of the following cell surface phenotype: CD8$^+$ CD44^{LO} CD62L^{HI} Qa2^{HI} and excluding a viability dye. For the peptide stimulation of P14 cells in vitro, naive P14 cells were sorted on the basis of the following cell surface phenotype: CD8$^+$ CD44^{LO} CD62L^{HI} Qa2^{HI} and excluding a viability dye. Unless otherwise stated, GFP^{LO} and GFP^{HI} cells are defined as the 10% of naive T cells with the lowest and highest GFP fluorescence intensity, respectively. For the DNA hairpin tension probe experiment, GFP^{LO} and GFP^{HI} cells were isolated from bulk OT-I T cells that were sorted on the basis of the following cell surface phenotype: CD4$^-$ CD19$^-$ and excluding a viability dye. The purity of CD8$^+$ T cells after enrichment was >96%.

Adoptive transfer and infections

For the polyclonal Nur77-GFP stability experiment, 5×10^5 GFP^{LO} or GFP^{HI} CD8$^+$ T cells were injected intravenously into congenic WT recipients in 200 μl of PBS. For the OT-I Nur77-GFP stability experiment, 1.3×10^6 to 1.8×10^6 naive GFP^{LO} or GFP^{HI} OT-I cells were injected intravenously into congenic WT recipients in 200 μl of PBS. In this experiment, GFP^{LO} and GFP^{HI} were defined as the 20% of naive OT-I cells with the lowest and highest GFP fluorescence intensity, respectively. Flow cytometry analysis was conducted 7 days (for polyclonal experiments) or 4 weeks (for OT-I experiments) later on CD8$^+$ T cells enriched from the spleen and lymph nodes. For adoptive transfers into *B2m*$^{-/-}$ or *B2m*$^{+/+}$ recipients, 2.2×10^6 to 2.5×10^6 naive CD44^{LO} CD62L^{HI} polyclonal CD8$^+$ T cells from Nur77-GFP-CD45.1 mice were injected intravenously in 200 μl of PBS. Flow cytometry analysis was conducted 10 days later on CD8$^+$ T cells enriched from the spleen and lymph nodes.

For the cotransfer experiment of P14 cells, GFP^{LO} and GFP^{HI} P14 cells were sorted from TCR Vα2$^+$ CD44^{LO} CD62L^{HI} Qa2^{HI} CD8$^+$ T cells. Three thousand congenically distinct GFP^{LO} and GFP^{HI} cells were coinjected intravenously in 200 μl of PBS into CD45.1$^+$ WT recipients (donor cells were either CD45.1$^+$ CD45.2$^+$ or CD45.2$^+$). Recipients were infected with 2×10^5 plaque-forming units (PFU) of LCMV Armstrong intraperitoneally the following day, and flow cytometry analysis was conducted 5 days later on splenic cells.

T cell stimulation

For in vitro stimulation of T cells, 5×10^4 sorted CD8$^+$ T cells were cultured with 2.5×10^5 APCs (T cell–depleted splenocytes) per well in a 96-well U-bottom plate. Polyclonal CD8$^+$ T cells were incubated with anti-CD3ε antibodies (0.25 μg/ml; clone 145-2C11) for 24 hours, whereas OT-I cells were incubated with SIINFEKL (N4) or SIIQFERL (Q4R7) or SIIGFEKL (G4) peptides (GenScript) at the indicated concentrations for 16 hours, and P14 cells were incubated with 10 nM GP33 (KAVYNFATC) for 16 hours. For OT-I

peptide titrations, log(agonist) versus response variable slope (four parameters) curves were fitted to the N4 and Q4R7 data. A log(agonist) versus response (three parameters) curve was fitted to the G4 data. As a positive control of TCR internalization, splenocytes were incubated with anti-CD3ε antibodies (10 μg/ml) and anti-CD28 antibodies (2 μg/ml; clone E18) for 90 min at 37°C before staining. Cells were cultured in RPMI 1640 (Thermo Fisher Scientific) supplemented with 10% fetal bovine serum (FBS), 1% penicillin-streptomycin-glutamine, 1% nonessential amino acids, 10 mM Hepes, 1 mM sodium pyruvate, and 50 μM 2-mercaptoethanol at 37°C with 5% CO_2.

Cytokine secretion assay

To detect IFN-γ secretion by stimulated polyclonal $CD8^+$ T cells, we used the IFN-γ Secretion Assay Kit (Miltenyi Biotec, catalog no. 130-090-984) after 24 hours of stimulation with APCs and peptide. IFN-γ– and IL-2–secreting OT-I cells were colabeled using the IFN-γ Secretion Assay Kit (Miltenyi Biotec, catalog no.130-090-516) and the IL-2 Secretion Assay Kit (Miltenyi Biotec, catalog no. 130-090-987) after 16 hours of stimulation. Briefly, 1×10^5 to 1.5×10^5 T cells, including cocultured T cell–depleted splenocytes, were labeled with the bispecific catch reagent and incubated in 50 ml of prewarmed RPMI supplemented with 10% FBS for 45 min at 37°C. Fifty-milliliter conical tubes were inverted every 5 min several times during incubation. After washing, cells were stained with the cytokine detection antibody/antibodies in addition to surface antibodies.

Ca^{2+} analysis

OT-I cells were labeled with 1.5 μM Indo-1 AM dye (Thermo Fisher Scientific) according to the manufacturer's instructions. APCs (T cell–depleted splenocytes) were pulsed for 30 min at 37°C with 1 μM SIINFEKL peptide and washed. All cells were incubated at 37°C during the acquisition and for 5 min before the start of the experiment. After the baseline Ca^{2+} levels of 4×10^6 OT-I cells were recorded for 30 s, cells were pipetted into an Eppendorf tube containing 8×10^6 peptide-pulsed APCs and spun down for 5 s in a microcentrifuge. The acquisition was resumed after the cell pellet was resuspended. The ratio of bound dye (Indo-violet) to unbound dye (Indo-blue) was analyzed for viable $CD8^+$ $CD44^{LO}$ GFP^{LO} and GFP^{HI} cells.

Preparation of tension probe surfaces

No. 1.5H glass coverslips (Ibidi) were placed in a rack and sequentially sonicated in Milli-Q water (18.2 megohms/cm) and ethanol for 10 min. The glass slides were then rinsed with Milli-Q water and immersed in freshly prepared piranha solution (3:1 sulfuric acid:H_2O_2) for 30 min. The cleaned substrates were rinsed with Milli-Q water at least six times in a 200-ml beaker and washed three times with ethanol. Slides were then incubated with 3% 3-aminopropyltriethoxysilane in 200 ml of ethanol for 1 hour, after which the surfaces were washed with ethanol three times and baked in an oven at 100°C for 30 min. The slides were then mounted onto a six-channel microfluidic cell (Sticky-Slide VI 0.4, Ibidi). To each channel, ~50 ml of *N*-hydroxysuccinimide (NHS)–polyethylene glycol $(PEG)_4$–azide (10 mg/ml) in 0.1 M $NaHCO_3$ (pH 9) was added and incubated for 1 hour. The channels were washed with 1 ml of Milli-Q water three times, and the remaining water in the channel was removed by pipetting. The surfaces were then blocked with 0.1% BSA for 30 min and washed with PBS three times. Subsequently, the hairpin tension probes were assembled in 1 M NaCl by mixing the Atto647N-biotin–labeled ligand strand (220 nM), the dibenzocyclooctyne (DBCO)-BHQ2–labeled quencher strand (220 nM), and the hairpin strand (200 nM) in the ratio of 1.1:1.1:1. The mixture was heat-annealed at 95°C for 5 min and cooled down to 25°C over a 30-min time window. The assembled probe (~50 ml) was added to the channels (at a final concentration of 100 nM) and incubated overnight at room temperature. This strategy allows for covalent immobilization of the tension probes on azide-modified substrates by strain-promoted cycloaddition reaction. Unbound DNA probes were washed away by PBS the next day. Streptavidin (10 mg/ml) was added to the channels and incubated for 45 min. After washes with PBS, a biotinylated pMHC (OVA N4-$H2K^b$) ligand (10 mg/ml) was added to the surfaces, incubated for 45 min, and washed with PBS. Surfaces were buffer-exchanged with Hanks' balanced salt solution before imaging.

Imaging TCR tension with DNA hairpin tension probes

TCR:pMHC interactions exert force and mechanically unfold the DNA hairpin, leading to the dye's (Atto647N-BHQ2) dequenching. T cells were added to the tension probe surface and incubated for 20 min at room temperature. Locking strand (200 nM) was added to the surface for 10 min to capture the tension signal.

Relative 2D affinity assay

Negative enrichment of $CD8^+$ T cells from OT-I-Nur77-GFP-*Trac*$^{-/-}$ spleens was performed using the CD8α$^+$ T Cell Isolation Kit (Miltenyi Biotec) according to the manufacturer's instructions. Naive GFP^{LO} and GFP^{HI} OT-I cells were sorted from viable $CD44^{LO}$ $CD62L^{HI}$ $Qa2^{HI}$ cells. To prevent CD8 co-receptor binding to MHC, monomers with an H-$2K^b$ a3 domain with a human leukocyte antigen (HLA)–A2 a3 domain were generated. The 2D-MP assay was performed as previously described (*28*, *98*, *99*). Briefly, human RBCs coated with various concentrations of biotin-LC-NHS (succinimidyl 6-(biotinamido)hexanoate, BioVision) were also coated with streptavidin (0.5 mg/ml) (Thermo Fisher Scientific) and then incubated with 1 μg of SIINFEKL (N4) or SIIVFEKL (V4) monomer generated by the National Institutes of Health Tetramer Core Facility. Surface pMHC and TCR densities were determined by flow cytometry using anti–TCR-β phycoerythrin (PE) antibody (BD Biosciences) and anti-mouse β2-microglobulin PE antibody (BioLegend) with BD QuantiBRITE PE beads for standardization (BD Biosciences). TCR:pMHC affinity calculations were determined as previously described (*28*, *98*).

RNA-seq analysis

$CD8^+$ $CD44^{LO}$ $CD62L^{HI}$ $Qa2^{HI}$ OT-I GFP^{LO} and GFP^{HI} cells (1×10^5) from three biological replicates were sorted into RLT Lysis Buffer (Qiagen) containing 1% 2-mercaptoethanol. RNA was isolated using the Zymo Quick-RNA MicroPrep kit (Zymo Research), complementary DNA was prepared from 1000-cell equivalent of RNA using the SMART-Seq v4 Ultra Low Input RNA Kit for Sequencing (Takara Bio), and next-generation sequencing libraries were generated using a Nextera XT DNA Library Preparation kit (Illumina). The library size patterning from a 2100 Bioanalyzer (Agilent) and the DNA concentration were used as quality control metrics of the generated libraries. Samples were sequenced at the Emory Nonhuman

Primate Genomics Core on NovaSeq6000 (Illumina) using PE100. FastQC (https://bioinformatics.babraham.ac.uk/projects/fastqc/) was used to validate the quality of sequencing reads. Adapter sequences were trimmed using Skewer, and reads were mapped to the mm10 genome using STAR (*100*, *101*). Duplicate reads were identified using PICARD (http://broadinstitute.github.io/picard/) and removed from the subsequent analyses. Reads mapping to exons were counted using the R package GenomicRanges (*102*). Genes were considered expressed if three reads per million were detected in all samples of at least one experimental group.

Analysis of DEGs was conducted in R v.4.1.1 using the edgeR package v.3.36.0 (*103*). Genes were considered differentially expressed at a Benjamini-Hochberg FDR-corrected *P* value of <0.05. Heatmaps were generated using the ComplexHeatmap v.2.10.0 R package (*104*). Venn diagrams were generated using the ggvenn package (https://CRAN.R-project.org/package=ggvenn). Pre-ranked GSEA was conducted using the GSEA tool v.4.2.3 (*105*). The ranked list of all detected transcripts was generated by multiplying the sign of the fold change by the $-\log_{10}$ of the *P* value. All other RNA sequencing plots were generated using the ggplot2 v.3.3.5 R package (*106*).

Statistical analysis

All statistical analyses were performed in Prism v.9.4.1 (GraphPad) or R v.4.1.1. A *P* value of <0.05 was considered significant. Details about the statistical tests used are available in each figure legend. The sample sizes of experiments were determined on the basis of preliminary or prior experiments with $CD4^+$ T cells that yielded significant results. No power analyses to calculate sample sizes were performed.

Supplementary Materials

This PDF file includes:

Figs. S1 to S6
Table S1
Reference (*109*)

Other Supplementary Material for this manuscript includes the following:

MDAR Reproducibility Checklist

REFERENCES AND NOTES

1. A. H. Courtney, W. L. Lo, A. Weiss, TCR signaling: Mechanisms of initiation and propagation. *Trends Biochem. Sci.* **43**, 108–123 (2018).
2. K. Kelly, U. Siebenlist, Immediate-early genes induced by antigen receptor stimulation. *Curr. Opin. Immunol.* **7**, 327–332 (1995).
3. D. R. Myers, J. Zikherman, J. P. Roose, Tonic signals: Why do lymphocytes bother? *Trends Immunol.* **38**, 844–857 (2017).
4. I. Stefanova, J. R. Dorfman, R. N. Germain, Self-recognition promotes the foreign antigen sensitivity of naive T lymphocytes. *Nature* **420**, 429–434 (2002).
5. N. S. van Oers, N. Killeen, A. Weiss, ZAP-70 is constitutively associated with tyrosine-phosphorylated TCR ζ in murine thymocytes and lymph node T cells. *Immunity* **1**, 675–685 (1994).
6. D. Rogers, A. Sood, H. Wang, J. J. P. van Beek, T. J. Rademaker, P. Artusa, C. Schneider, C. Shen, D. C. Wong, A. Bhagrath, M. E. Lebel, S. A. Condotta, M. J. Richer, A. J. Martins, J. S. Tsang, L. B. Barreiro, P. Francois, D. Langlais, H. J. Melichar, J. Textor, J. N. Mandl, Pre-existing chromatin accessibility and gene expression differences among naive $CD4^+$ T cells influence effector potential. *Cell Rep.* **37**, 110064 (2021).
7. W. M. Zinzow-Kramer, E. M. Kolawole, J. Eggert, B. D. Evavold, C. D. Scharer, B. B. Au-Yeung, Strong basal/tonic TCR signals are associated with negative regulation of naive $CD4^+$ T cells. *Immunohorizons* **6**, 671–683 (2022).
8. S. This, D. Rogers, E. Mallet Gauthier, J. N. Mandl, H. J. Melichar, What's self got to do with it: Sources of heterogeneity among naive T cells. *Semin. Immunol.* **65**, 101702 (2022).
9. D. R. Myers, T. Lau, E. Markegard, H. W. Lim, H. Kasler, M. Zhu, A. Barczak, J. P. Huizar, J. Zikherman, D. J. Erle, W. Zhang, E. Verdin, J. P. Roose, Tonic LAT-HDAC7 signals sustain *Nur77* and *Irf4* expression to tune naive CD4 T cells. *Cell Rep.* **19**, 1558–1571 (2017).
10. J. Eggert, B. B. Au-Yeung, Functional heterogeneity and adaptation of naive T cells in response to tonic TCR signals. *Curr. Opin. Immunol.* **73**, 43–49 (2021).
11. A. C. Richard, Divide and conquer: Phenotypic and temporal heterogeneity within $CD8^+$ T cell responses. *Front. Immunol.* **13**, 949423 (2022).
12. E. Jennings, T. A. E. Elliot, N. Thawait, S. Kanabar, J. C. Yam-Puc, M. Ono, K. M. Toellner, D. C. Wraith, G. Anderson, D. Bending, Nr4a1 and Nr4a3 reporter mice are differentially sensitive to T cell receptor signal strength and duration. *Cell Rep.* **33**, 108328 (2020).
13. A. E. Moran, K. L. Holzapfel, Y. Xing, N. R. Cunningham, J. S. Maltzman, J. Punt, K. A. Hogquist, T cell receptor signal strength in T_{reg} and iNKT cell development demonstrated by a novel fluorescent reporter mouse. *J. Exp. Med.* **208**, 1279–1289 (2011).
14. J. Zikherman, R. Parameswaran, A. Weiss, Endogenous antigen tunes the responsiveness of naive B cells but not T cells. *Nature* **489**, 160–164 (2012).
15. B. B. Au-Yeung, G. A. Smith, J. L. Mueller, C. S. Heyn, R. G. Jaszczak, A. Weiss, J. Zikherman, IL-2 modulates the TCR signaling threshold for CD8 but Not CD4 T cell proliferation on a single-cell level. *J. Immunol.* **198**, 2445–2456 (2017).
16. B. B. Au-Yeung, J. Zikherman, J. L. Mueller, J. F. Ashouri, M. Matloubian, D. A. Cheng, Y. Chen, K. M. Shokat, A. Weiss, A sharp T-cell antigen receptor signaling threshold for T-cell proliferation. *Proc. Natl. Acad. Sci. U.S.A.* **111**, E3679–E3688 (2014).
17. J. R. Dorfman, I. Stefanova, K. Yasutomo, R. N. Germain, $CD4^+$ T cell survival is not directly linked to self-MHC-induced TCR signaling. *Nat. Immunol.* **1**, 329–335 (2000).
18. W. M. Zinzow-Kramer, A. Weiss, B. B. Au-Yeung, Adaptation by naïve $CD4^+$T cells to self-antigen-dependent TCR signaling induces functional heterogeneity and tolerance. *Proc. Natl. Acad. Sci. U.S.A.* **116**, 15160–15169 (2019).
19. H. M. Lee, J. L. Bautista, J. Scott-Browne, J. F. Mohan, C. S. Hsieh, A broad range of self-reactivity drives thymic regulatory T cell selection to limit responses to self. *Immunity* **37**, 475–486 (2012).
20. M. Hinterberger, M. Aichinger, O. Prazeres da Costa, D. Voehringer, R. Hoffmann, L. Klein, Autonomous role of medullary thymic epithelial cells in central $CD4^+$ T cell tolerance. *Nat. Immunol.* **11**, 512–519 (2010).
21. M. S. Jordan, A. Boesteanu, A. J. Reed, A. L. Petrone, A. E. Holenbeck, M. A. Lerman, A. Naji, A. J. Caton, Thymic selection of $CD4^+CD25^+$ regulatory T cells induced by an agonist self-peptide. *Nat. Immunol.* **2**, 301–306 (2001).
22. J. N. Mandl, J. P. Monteiro, N. Vrisekoop, R. N. Germain, T cell-positive selection uses self-ligand binding strength to optimize repertoire recognition of foreign antigens. *Immunity* **38**, 263–274 (2013).
23. J. H. Cho, H. O. Kim, Y. J. Ju, Y. C. Kye, G. W. Lee, S. W. Lee, C. H. Yun, N. Bottini, K. Webster, C. C. Goodnow, C. D. Surh, C. King, J. Sprent, CD45-mediated control of TCR tuning in naïve and memory $CD8^+$ T cells. *Nat. Commun.* **7**, 13373 (2016).
24. H. S. Azzam, A. Grinberg, K. Lui, H. Shen, E. W. Shores, P. E. Love, CD5 expression is developmentally regulated by T cell receptor (TCR) signals and TCR avidity. *J. Exp. Med.* **188**, 2301–2311 (1998).
25. H. S. Azzam, J. B. DeJarnette, K. Huang, R. Emmons, C. S. Park, C. L. Sommers, D. El-Khoury, E. W. Shores, P. E. Love, Fine tuning of TCR signaling by CD5. *J. Immunol.* **166**, 5464–5472 (2001).
26. P. Wong, G. M. Barton, K. A. Forbush, A. Y. Rudensky, Dynamic tuning of T cell reactivity by self-peptide-major histocompatibility complex ligands. *J. Exp. Med.* **193**, 1179–1187 (2001).
27. R. B. Fulton, S. E. Hamilton, Y. Xing, J. A. Best, A. W. Goldrath, K. A. Hogquist, S. C. Jameson, The TCR's sensitivity to self peptide-MHC dictates the ability of naive $CD8^+$ T cells to respond to foreign antigens. *Nat. Immunol.* **16**, 107–117 (2015).
28. J. Huang, V. I. Zarnitsyna, B. Liu, L. J. Edwards, N. Jiang, B. D. Evavold, C. Zhu, The kinetics of two-dimensional TCR and pMHC interactions determine T-cell responsiveness. *Nature* **464**, 932–936 (2010).
29. T. E. Boursalian, J. Golob, D. M. Soper, C. J. Cooper, P. J. Fink, Continued maturation of thymic emigrants in the periphery. *Nat. Immunol.* **5**, 418–425 (2004).
30. E. M. Kolawole, T. J. Lamb, B. D. Evavold, Relationship of 2D affinity to T cell functional outcomes. *Int. J. Mol. Sci.* **21**, 7969 (2020).
31. V. I. Zarnitsyna, C. Zhu, Adhesion frequency assay for in situ kinetics analysis of cross-junctional molecular interactions at the cell-cell interface. *J. Vis. Exp.* , e3519 (2011).
32. P. Corish, C. Tyler-Smith, Attenuation of green fluorescent protein half-life in mammalian cells. *Protein Eng.* **12**, 1035–1040 (1999).
33. A. Sacchetti, T. El Sewedy, A. F. Nasr, S. Alberti, Efficient GFP mutations profoundly affect mRNA transcription and translation rates. *FEBS Lett.* **492**, 151–155 (2001).
34. R. Manz, M. Assenmacher, E. Pfluger, S. Miltenyi, A. Radbruch, Analysis and sorting of live cells according to secreted molecules, relocated to a cell-surface affinity matrix. *Proc. Natl. Acad. Sci. U.S.A.* **92**, 1921–1925 (1995).
35. J. D. Campbell, Detection and enrichment of antigen-specific $CD4^+$ and $CD8^+$ T cells based on cytokine secretion. *Methods* **31**, 150–159 (2003).

36. J. J. Bird, D. R. Brown, A. C. Mullen, N. H. Moskowitz, M. A. Mahowald, J. R. Sider, T. F. Gajewski, C. R. Wang, S. L. Reiner, Helper T cell differentiation is controlled by the cell cycle. *Immunity* **9**, 229–237 (1998).
37. A. V. Gett, P. D. Hodgkin, Cell division regulates the T cell cytokine repertoire, revealing a mechanism underlying immune class regulation. *Proc. Natl. Acad. Sci. U.S.A.* **95**, 9488–9493 (1998).
38. J. L. Grogan, M. Mohrs, B. Harmon, D. A. Lacy, J. W. Sedat, R. M. Locksley, Early transcription and silencing of cytokine genes underlie polarization of T helper cell subsets. *Immunity* **14**, 205–215 (2001).
39. Y. Laouar, I. N. Crispe, Functional flexibility in T cells: Independent regulation of $CD4^+$ T cell proliferation and effector function in vivo. *Immunity* **13**, 291–301 (2000).
40. E. N. Kersh, D. R. Fitzpatrick, K. Murali-Krishna, J. Shires, S. H. Speck, J. M. Boss, R. Ahmed, Rapid demethylation of the IFN-γ gene occurs in memory but not naive CD8 T cells. *J. Immunol.* **176**, 4083–4093 (2006).
41. N. Auphan-Anezin, G. Verdeil, A. M. Schmitt-Verhulst, Distinct thresholds for CD8 T cell activation lead to functional heterogeneity: CD8 T cell priming can occur independently of cell division. *J. Immunol.* **170**, 2442–2448 (2003).
42. S. R. Achar, F. X. P. Bourassa, T. J. Rademaker, A. Lee, T. Kondo, E. Salazar-Cavazos, J. S. Davies, N. Taylor, P. Francois, G. Altan-Bonnet, Universal antigen encoding of T cell activation from high-dimensional cytokine dynamics. *Science* **376**, 880–884 (2022).
43. P. Wolint, M. R. Betts, R. A. Koup, A. Oxenius, Immediate cytotoxicity but not degranulation distinguishes effector and memory subsets of $CD8^+$ T cells. *J. Exp. Med.* **199**, 925–936 (2004).
44. H. Pircher, D. Moskophidis, U. Rohrer, K. Burki, H. Hengartner, R. M. Zinkernagel, Viral escape by selection of cytotoxic T cell-resistant virus variants in vivo. *Nature* **346**, 629–633 (1990).
45. M. A. Daniels, E. Teixeiro, J. Gill, B. Hausmann, D. Roubaty, K. Holmberg, G. Werlen, G. A. Hollander, N. R. Gascoigne, E. Palmer, Thymic selection threshold defined by compartmentalization of Ras/MAPK signalling. *Nature* **444**, 724–729 (2006).
46. M. A. Al-Aghbar, A. K. Jainarayanan, M. L. Dustin, S. R. Roffler, The interplay between membrane topology and mechanical forces in regulating T cell receptor activity. *Commun. Biol.* **5**, 40 (2022).
47. Y. Liu, L. Blanchfield, V. P. Ma, R. Andargachew, K. Galior, Z. Liu, B. Evavold, K. Salaita, DNA-based nanoparticle tension sensors reveal that T-cell receptors transmit defined pN forces to their antigens for enhanced fidelity. *Proc. Natl. Acad. Sci. U.S.A.* **113**, 5610–5615 (2016).
48. R. Ma, A. V. Kellner, V. P. Ma, H. Su, B. R. Deal, J. M. Brockman, K. Salaita, DNA probes that store mechanical information reveal transient piconewton forces applied by T cells. *Proc. Natl. Acad. Sci. U.S.A.* **116**, 16949–16954 (2019).
49. K. Man, M. Miasari, W. Shi, A. Xin, D. C. Henstridge, S. Preston, M. Pellegrini, G. T. Belz, G. K. Smyth, M. A. Febbraio, S. L. Nutt, A. Kallies, The transcription factor IRF4 is essential for TCR affinity-mediated metabolic programming and clonal expansion of T cells. *Nat. Immunol.* **14**, 1155–1165 (2013).
50. J. M. Conley, M. P. Gallagher, A. Rao, L. J. Berg, Activation of the Tec kinase ITK controls graded IRF4 expression in response to variations in TCR signal strength. *J. Immunol.* **205**, 335–345 (2020).
51. C. J. Luckey, D. Bhattacharya, A. W. Goldrath, I. L. Weissman, C. Benoist, D. Mathis, Memory T and memory B cells share a transcriptional program of self-renewal with long-term hematopoietic stem cells. *Proc. Natl. Acad. Sci. U.S.A.* **103**, 3304–3309 (2006).
52. J. A. Best, D. A. Blair, J. Knell, E. Yang, V. Mayya, A. Doedens, M. L. Dustin, A. W. Goldrath, The Immunological Genome Project Consortium, Transcriptional insights into the $CD8^+$ T cell response to infection and memory T cell formation. *Nat. Immunol.* **14**, 404–412 (2013).
53. J. T. White, E. W. Cross, M. A. Burchill, T. Danhorn, M. D. McCarter, H. R. Rosen, B. O'Connor, R. M. Kedl, Virtual memory T cells develop and mediate bystander protective immunity in an IL-15-dependent manner. *Nat. Commun.* **7**, 11291 (2016).
54. S. M. Kaech, W. Cui, Transcriptional control of effector and memory $CD8^+$ T cell differentiation. *Nat. Rev. Immunol.* **12**, 749–761 (2012).
55. F. Alfei, K. Kanev, M. Hofmann, M. Wu, H. E. Ghoneim, P. Roelli, D. T. Utzschneider, M. von Hoesslin, J. G. Cullen, Y. Fan, V. Eisenberg, D. Wohlleber, K. Steiger, D. Merkler, M. Delorenzi, P. A. Knolle, C. J. Cohen, R. Thimme, B. Youngblood, D. Zehn, TOX reinforces the phenotype and longevity of exhausted T cells in chronic viral infection. *Nature* **571**, 265–269 (2019).
56. F. Miyagawa, H. Zhang, A. Terunuma, K. Ozato, Y. Tagaya, S. I. Katz, Interferon regulatory factor 8 integrates T-cell receptor and cytokine-signaling pathways and drives effector differentiation of CD8 T cells. *Proc. Natl. Acad. Sci. U.S.A.* **109**, 12123–12128 (2012).
57. K. E. Pollok, Y. J. Kim, Z. Zhou, J. Hurtado, K. K. Kim, R. T. Pickard, B. S. Kwon, Inducible T cell antigen 4-1BB. Analysis of expression and function. *J. Immunol.* **150**, 771–781 (1993).
58. K. E. Pollok, S. H. Kim, B. S. Kwon, Regulation of 4-1BB expression by cell-cell interactions and the cytokines, interleukin-2 and interleukin-4. *Eur. J. Immunol.* **25**, 488–494 (1995).
59. B. R. Wong, J. Rho, J. Arron, E. Robinson, J. Orlinick, M. Chao, S. Kalachikov, E. Cayani, F. S. Bartlett III, W. N. Frankel, S. Y. Lee, Y. Choi, TRANCE is a novel ligand of the tumor necrosis factor receptor family that activates c-Jun N-terminal kinase in T cells. *J. Biol. Chem.* **272**, 25190–25194 (1997).
60. R. J. Snelgrove, J. Goulding, A. M. Didierlaurent, D. Lyonga, S. Vekaria, L. Edwards, E. Gwyer, J. D. Sedgwick, A. N. Barclay, T. Hussell, A critical function for CD200 in lung immune homeostasis and the severity of influenza infection. *Nat. Immunol.* **9**, 1074–1083 (2008).
61. C. Lutz-Nicoladoni, D. Wolf, S. Sopper, Modulation of immune cell functions by the E3 ligase Cbl-b. *Front. Oncol.* **5**, 58 (2015).
62. J. N. Mandl, R. Liou, F. Klauschen, N. Vrisekoop, J. P. Monteiro, A. J. Yates, A. Y. Huang, R. N. Germain, Quantification of lymph node transit times reveals differences in antigen surveillance strategies of naive $CD4^+$ and $CD8^+$ T cells. *Proc. Natl. Acad. Sci. U.S.A.* **109**, 18036–18041 (2012).
63. T. A. E. Elliot, E. K. Jennings, D. A. J. Lecky, S. Rouvray, G. M. Mackie, L. Scarfe, L. Sheriff, M. Ono, K. M. Maslowski, D. Bending, Nur77-Tempo mice reveal T cell steady state antigen recognition. *Discov. Immunol.* **1**, kyac009 (2022).
64. D. Bending, P. Prieto Martin, A. Paduraru, C. Ducker, E. Marzaganov, M. Laviron, S. Kitano, H. Miyachi, T. Crompton, M. Ono, A timer for analyzing temporally dynamic changes in transcription during differentiation in vivo. *J. Cell Biol.* **217**, 2931–2950 (2018).
65. J. O. Ross, H. J. Melichar, B. B. Au-Yeung, P. Herzmark, A. Weiss, E. A. Robey, Distinct phases in the positive selection of $CD8^+$ T cells distinguished by intrathymic migration and T-cell receptor signaling patterns. *Proc. Natl. Acad. Sci. U.S.A.* **111**, E2550–E2558 (2014).
66. B. B. Au-Yeung, H. J. Melichar, J. O. Ross, D. A. Cheng, J. Zikherman, K. M. Shokat, E. A. Robey, A. Weiss, Quantitative and temporal requirements revealed for Zap70 catalytic activity during T cell development. *Nat. Immunol.* **15**, 687–694 (2014).
67. A. Trefzer, P. Kadam, S. H. Wang, S. Pennavaria, B. Lober, B. Akcabozan, J. Kranich, T. Brocker, N. Nakano, M. Irmler, J. Beckers, T. Straub, R. Obst, Dynamic adoption of anergy by antigen-exhausted $CD4^+$ T cells. *Cell Rep.* **34**, 108748 (2021).
68. T. T. T. Nguyen, Z. E. Wang, L. Shen, A. Schroeder, W. Eckalbar, A. Weiss, Cbl-b deficiency prevents functional but not phenotypic T cell anergy. *J. Exp. Med.* **218**, e20202477 (2021).
69. G. Qiao, Z. Li, L. Molinero, M. L. Alegre, H. Ying, Z. Sun, J. M. Penninger, J. Zhang, T-cell receptor-induced NF-κB activation is negatively regulated by E3 ubiquitin ligase Cbl-b. *Mol. Cell. Biol.* **28**, 2470–2480 (2008).
70. K. Bachmaier, C. Krawczyk, I. Kozieradzki, Y. Y. Kong, T. Sasaki, A. Oliveira-dos-Santos, S. Mariathasan, D. Bouchard, A. Wakeham, A. Itie, J. Le, P. S. Ohashi, I. Sarosi, H. Nishina, S. Lipkowitz, J. M. Penninger, Negative regulation of lymphocyte activation and autoimmunity by the molecular adaptor Cbl-b. *Nature* **403**, 211–216 (2000).
71. G. Voisinne, A. Garcia-Blesa, K. Chaoui, F. Fiore, E. Bergot, L. Girard, M. Malissen, O. Burlet-Schiltz, A. Gonzalez de Peredo, B. Malissen, R. Roncagalli, Co-recruitment analysis of the CBL and CBLB signalosomes in primary T cells identifies CD5 as a key regulator of TCR-induced ubiquitylation. *Mol. Syst. Biol.* **12**, 876 (2016).
72. A. Mikhailik, B. Ford, J. Keller, Y. Chen, N. Nassar, N. Carpino, A phosphatase activity of Sts-1 contributes to the suppression of TCR signaling. *Mol. Cell* **27**, 486, 497 (2007).
73. L. Odagiu, J. May, S. Boulet, T. A. Baldwin, N. Labrecque, Role of the orphan nuclear receptor NR4A family in T-cell biology. *Front. Endocrinol.* **11**, 624122 (2020).
74. X. Liu, Y. Wang, H. Lu, J. Li, X. Yan, M. Xiao, J. Hao, A. Alekseev, H. Khong, T. Chen, R. Huang, J. Wu, Q. Zhao, Q. Wu, S. Xu, X. Wang, W. Jin, S. Yu, Y. Wang, L. Wei, A. Wang, B. Zhong, L. Ni, X. Liu, R. Nurieva, L. Ye, Q. Tian, X. W. Bian, C. Dong, Genome-wide analysis identifies NR4A1 as a key mediator of T cell dysfunction. *Nature* **567**, 525–529 (2019).
75. M. Liebmann, S. Hucke, K. Koch, M. Eschborn, J. Ghelman, A. I. Chasan, S. Glander, M. Schadlich, M. Kuhlencord, N. M. Daber, M. Eveslage, M. Beyer, M. Dietrich, P. Albrecht, M. Stoll, K. B. Busch, H. Wiendl, J. Roth, T. Kuhlmann, L. Klotz, Nur77 serves as a molecular brake of the metabolic switch during T cell activation to restrict autoimmunity. *Proc. Natl. Acad. Sci. U.S.A.* **115**, E8017–E8026 (2018).
76. R. Hiwa, H. V. Nielsen, J. L. Mueller, R. Mandla, J. Zikherman, NR4A family members regulate T cell tolerance to preserve immune homeostasis and suppress autoimmunity. *JCI Insight* **6**, e151005 (2021).
77. J. Chen, I. F. Lopez-Moyado, H. Seo, C. J. Lio, L. J. Hempleman, T. Sekiya, A. Yoshimura, J. P. Scott-Browne, A. Rao, NR4A transcription factors limit CAR T cell function in solid tumours. *Nature* **567**, 530–534 (2019).
78. D. Bending, J. Zikherman, Nr4a nuclear receptors: Markers and modulators of antigen receptor signaling. *Curr. Opin. Immunol.* **81**, 102285 (2023).
79. N. Carpino, S. Turner, D. Mekala, Y. Takahashi, H. Zang, T. L. Geiger, P. Doherty, J. N. Ihle, Regulation of ZAP-70 activation and TCR signaling by two related proteins, Sts-1 and Sts-2. *Immunity* **20**, 37–46 (2004).
80. S. M. Stanford, N. Rapini, N. Bottini, Regulation of TCR signalling by tyrosine phosphatases: From immune homeostasis to autoimmunity. *Immunology* **137**, 1–19 (2012).
81. J. P. Li, C. Y. Yang, H. C. Chuang, J. L. Lan, D. Y. Chen, Y. M. Chen, X. Wang, A. J. Chen, J. W. Belmont, T. H. Tan, The phosphatase JKAP/DUSP22 inhibits T-cell receptor signalling and autoimmunity by inactivating Lck. *Nat. Commun.* **5**, 3618 (2014).

82. F. Wiede, N. L. La Gruta, T. Tiganis, PTPN2 attenuates T-cell lymphopenia-induced proliferation. *Nat. Commun.* **5**, 3073 (2014).
83. A. Tarakhovsky, S. B. Kanner, J. Hombach, J. A. Ledbetter, W. Muller, N. Killeen, K. Rajewsky, A role for CD5 in TCR-mediated signal transduction and thymocyte selection. *Science* **269**, 535–537 (1995).
84. C. Pena-Rossi, L. A. Zuckerman, J. Strong, J. Kwan, W. Ferris, S. Chan, A. Tarakhovsky, A. D. Beyers, N. Killeen, Negative regulation of CD4 lineage development and responses by CD5. *J. Immunol.* **163**, 6494–6501 (1999).
85. Y. J. Ju, S. W. Lee, Y. C. Kye, G. W. Lee, H. O. Kim, C. H. Yun, J. H. Cho, Self-reactivity controls functional diversity of naive $CD8^+$ T cells by co-opting tonic type I interferon. *Nat. Commun.* **12**, 6059 (2021).
86. E. S. Huseby, E. Teixeiro, The perception and response of T cells to a changing environment are based on the law of initial value. *Sci. Signal.* **15**, eabj9842 (2022).
87. Z. Grossman, W. E. Paul, Adaptive cellular interactions in the immune system: The tunable activation threshold and the significance of subthreshold responses. *Proc. Natl. Acad. Sci. U.S.A.* **89**, 10365–10369 (1992).
88. T. A. E. Elliot, E. K. Jennings, D. A. J. Lecky, N. Thawait, A. Flores-Langarica, A. Copland, K. M. Maslowski, D. C. Wraith, D. Bending, Antigen and checkpoint receptor engagement recalibrates T cell receptor signal strength. *Immunity* **54**, 2481–2496.e6 (2021).
89. V. R. Buchholz, T. N. Schumacher, D. H. Busch, T cell fate at the single-cell level. *Annu. Rev. Immunol.* **34**, 65–92 (2016).
90. H. S. Wong, R. N. Germain, Robust control of the adaptive immune system. *Semin. Immunol.* **36**, 17–27 (2018).
91. T. A. Kadlecek, N. S. van Oers, L. Lefrancois, S. Olson, D. Finlay, D. H. Chu, K. Connolly, N. Killeen, A. Weiss, Differential requirements for ZAP-70 in TCR signaling and T cell development. *J. Immunol.* **161**, 4688–4694 (1998).
92. Y. Y. Wan, R. A. Flavell et al., *Proc. Natl. Acad. Sci. U.S.A.* **102**, 5126–5131 (2005).
93. B. H. Koller, P. Marrack, J. W. Kappler, O. Smithies, Normal development of mice deficient in beta 2M, MHC class I proteins, and $CD8^+$ T cells. *Science* **248**, 1227–1230 (1990).
94. H. Pircher, E. E. Michalopoulos, A. Iwamoto, P. S. Ohashi, J. Baenziger, H. Hengartner, R. M. Zinkernagel, T. W. Mak, Molecular analysis of the antigen receptor of virus-specific cytotoxic T cells and identification of a new V α family. *Eur. J. Immunol.* **17**, 1843–1846 (1987).
95. Y. J. Chiang, H. K. Kole, K. Brown, M. Naramura, S. Fukuhara, R. J. Hu, I. K. Jang, J. S. Gutkind, E. Shevach, H. Gu, Cbl-b regulates the CD28 dependence of T-cell activation. *Nature* **403**, 216–220 (2000).
96. G. A. Smith, K. Uchida, A. Weiss, J. Taunton, Essential biphasic role for JAK3 catalytic activity in IL-2 receptor signaling. *Nat. Chem. Biol.* **12**, 373–379 (2016).
97. K. G. Anderson, H. Sung, C. N. Skon, L. Lefrancois, A. Deisinger, V. Vezys, D. Masopust, Cutting edge: Intravascular staining redefines lung CD8 T cell responses. *J. Immunol.* **189**, 2702–2706 (2012).
98. E. M. Kolawole, R. Andargachew, B. Liu, J. R. Jacobs, B. D. Evavold, 2D kinetic analysis of TCR and CD8 coreceptor for LCMV GP33 epitopes. *Front. Immunol.* **9**, 2348 (2018).
99. E. Evans, A. Leung, V. Heinrich, C. Zhu, Mechanical switching and coupling between two dissociation pathways in a P-selectin adhesion bond. *Proc. Natl. Acad. Sci. U.S.A.* **101**, 11281–11286 (2004).
100. A. Dobin, T. R. Gingeras, Mapping RNA-seq reads with STAR. *Curr. Protoc. Bioinformatics* **51**, 11.14.11–11.14.19 (2015).
101. H. Jiang, R. Lei, S. W. Ding, S. Zhu, Skewer: A fast and accurate adapter trimmer for next-generation sequencing paired-end reads. *BMC Bioinformatics* **15**, 182 (2014).
102. M. Lawrence, W. Huber, H. Pages, P. Aboyoun, M. Carlson, R. Gentleman, M. T. Morgan, V. J. Carey, Software for computing and annotating genomic ranges. *PLOS Comput. Biol.* **9**, e1003118 (2013).
103. M. D. Robinson, D. J. McCarthy, G. K. Smyth et al., *Bioinformatics* **26**, 139–140 (2010).
104. Z. Gu, R. Eils, M. Schlesner, Complex heatmaps reveal patterns and correlations in multidimensional genomic data. *Bioinformatics* **32**, 2847–2849 (2016).
105. A. Subramanian, P. Tamayo, V. K. Mootha, S. Mukherjee, B. L. Ebert, M. A. Gillette, A. Paulovich, S. L. Pomeroy, T. R. Golub, E. S. Lander, J. P. Mesirov, Gene set enrichment analysis: A knowledge-based approach for interpreting genome-wide expression profiles. *Proc. Natl. Acad. Sci. U.S.A.* **102**, 15545–15550 (2005).
106. H. Wickham, *Use R!* (Springer, 2016).
107. E. J. Wherry, S. J. Ha, S. M. Kaech, W. N. Haining, S. Sarkar, V. Kalia, S. Subramaniam, J. N. Blattman, D. L. Barber, R. Ahmed, Molecular signature of $CD8^+$ T cell exhaustion during chronic viral infection. *Immunity* **27**, 670–684 (2007).
108. I. A. Parish, S. Rao, G. K. Smyth, T. Juelich, G. S. Denyer, G. M. Davey, A. Strasser, W. R. Heath, The molecular signature of $CD8^+$ T cells undergoing deletional tolerance. *Blood* **113**, 4575–4585 (2009).
109. R. Ahmed, A. Salmi, L. D. Butler, J. M. Chiller, M. B. Oldstone, Selection of genetic variants of lymphocytic choriomeningitis virus in spleens of persistently infected mice. Role in suppression of cytotoxic T lymphocyte response and viral persistence. *J. Exp. Med.* **160**, 521–540 (1984).

Acknowledgments: We thank S. Grassmann and W.-L. Lo for critical reading of the manuscript. We also thank the Pediatric/Winship Flow Cytometry Core for cell sorting, the Emory Integrated Genomics Core (EIGC) for RNA-seq, and the NIH Tetramer Core Facility for providing pMHC tetramers. We would like to thank R. Ahmed for providing LCMV Armstrong virus, D. McManus for assistance with LCMV experiments, and Y. Liu for statistical consultation. **Funding:** This work was supported in part by National Institute of Allergy and Infectious Diseases R01AI165706 (B.B.A.-Y.) and R01AI172253 (B.D.E.), NCI T32 CA108462-17 (Y.-L.T.), and a Cancer Research Institute Irvington Postdoctoral Fellowship (Y.-L.T.). **Author contributions:** J.E. and B.B.A.-Y. conceptualized the study. J.E., W.M.Z.-K., B.B.A.-Y., Y.H., and E.M.K. performed experiments. J.E., W.M.Z.-K., and C.D.S. analyzed the RNA-seq data. K.S. and Y.H. designed and performed the tension probe experiments. E.M.K. and B.D.E. designed and performed the relative 2D affinity experiments. Y.-L.T. and A.W. contributed conceptual input and provided *Cblb*$^{-/-}$ and Nur77-GFP-*Cblb*$^{-/-}$ cells. J.E. and B.B.A.-Y. wrote the manuscript with input from all authors. B.B.A.-Y. supervised the study. **Competing interests:** A.W. is a cofounder and a scientific advisory board member of Nurix Therapeutics Inc., which has a Cbl-b inhibitor in phase 1 clinical trials. A.W. owns stock and receives consulting fees from Nurix. The other authors declare that they have no competing interests. **Data and materials availability:** RNA-seq data are available under the accession number GSE223457 in the Gene Expression Omnibus (https://ncbi.nlm.nih.gov/geo/query/acc.cgi?acc=GSE223457). All other data needed to evaluate the conclusions in the paper are present in the paper or the Supplementary Materials. The Nur77-GFP mouse strain has been donated to the Mutant Mouse Regional Resource Centers (MMRRC).

Submitted 7 February 2023
Resubmitted 26 June 2023
Accepted 18 January 2024
Published 6 February 2024
10.1126/scisignal.adh0439